Geophysical Journal International

Geophys. J. Int. (2019) **217,** 1089–1107
Advance Access publication 2019 February 06
GJI Geomagnetism, rock magnetism and palaeomagnetism

doi: 10.1093/gji/ggz075

Coring induced sediment fabrics at IODP Expedition 347 Sites M0061 and M0062 identified by anisotropy of magnetic susceptibility (AMS): criteria for accepting palaeomagnetic data

Ian Snowball,[1] Bjarne Almqvist,[1] Bryan C. Lougheed,[2] Steffen Wiers,[1] Stephen Obrochta[3] and Emilio Herrero-Bervera[4]

[1]*Department of Earth Sciences, Uppsala University, Sweden. E-mail: ian.snowball@geo.uu.se*
[2]*Laboratoire des Sciences du Climat et de l'Environment, LSCE/IPSL, Laboratoire CNRS-CEA-UVSQ, France*
[3]*Graduate School of International Resource Science, Akita University, Japan*
[4]*School of Ocean Earth Science and Technology (SOEST) within the Hawaii Institute of Geophysics and Planetology (HIGP) of the University of Hawaii at Manoa, Hawaii, USA*

Accepted 2019 February 5. Received 2019 January 30; in original form 2018 September 21

SUMMARY

Anisotropy of magnetic susceptibility data obtained from discrete subsamples recovered from two Integrated Ocean Drilling Program sites (Expedition 347 sites M0061 and M0062 in the Baltic Sea) by an Advanced Piston Corer are compared to results obtained on subsamples recovered by replicate 6-m-long Kullenberg piston cores. Characteristic natural remanence directions were obtained from the total of 1097 subsamples using principal component analyses. The three principal anisotropy axes of subsamples taken from Advanced Piston Core liners align to the subsample axes, with the maximum axis (K_1) parallel to the split core surfaces, possibly caused by outwards relaxation of the core-liners after splitting. A second anomalous anisotropy fabric is characterized by steep values of the angular difference between the inclination of the minimum anisotropy axes (K_3) and that expected for horizontal bedding (90°). This fabric is confined to the upper 1–2 m of the Kullenberg cores and specific sections of the advanced piston cores, and we attribute it to conical deformation caused by either excessive penetration speeds and downwards dragging of sediment along the edge of the liner or stretching caused by undersampling. By using our data in an example, we present a protocol to accept palaeomagnetic secular variation data that uses (i) a threshold 90-K_3 value of 15°, combined with a modelled, locally applicable minimum inclination of 65° and (ii) an A95 cone of confidence based on Fisher statistics applied to virtual geomagnetic pole distributions.

Key words: Magnetic fabrics and anisotropy; Palaeomagnetic secular variation; Palaeomagnetism.

1 INTRODUCTION

Since the late 1960s palaeomagnetic data sets covering much of the Earth's surface have been generated through studies of (post)-depositional remanent magnetizations (pDRMs) acquired by unconsolidated lacustrine and marine sediments (e.g. Turner & Thompson 1981; Haltia-Hovi *et al.* 2010; Barletta *et al.* 2010; Richter *et al.* 2006). Many published data sets have been incorporated into palaeomagnetic databases (e.g. GEOMAGIA50.v3 by Brown *et al.* 2015). These data are utilized in different ways, such as their amalgamation into regionally restricted PSV 'master curves' (e.g. Turner & Thompson 1981; Snowball *et al.* 2007; Lougheed *et al.* 2014) that can be used for relative dating (e.g. Stanton *et al.* 2010; Lougheed *et al.* 2014) or as constraints on time-varying geomagnetic field models of different complexities (e.g. Nilsson *et al.* 2014; Panovska *et al.* 2015; Hellio & Gillet 2018). Palaeomagnetic data are routinely acquired as part of international scientific drilling initiatives (e.g. IODP[1], ICDP[2]) in efforts to construct a site-specific geochronology based on correlation to the geomagnetic polarity timescale (GPTS) (Ogg & Smith 2004), accepted records of geomagnetic excursions (e.g. Channell *et al.* 2002), relative palaeointensity (e.g. Viglotti *et al.* 2014) and palaeomagnetic secular variation (PSV) (e.g. Lund *et al.* 2006).

Natural remanent magnetization (NRM) data obtained from sediments include known and unknown uncertainties that arise from

[1]International Ocean Discovery Program (which succeeded the Integrated Ocean Drilling Program).
[2]International Continental Scientific Drilling Program.

the natural magnetic recording processes, (sub)sampling methods and laboratory analyses. Central to all palaeomagnetic studies of unconsolidated sediments is the need to characterize the stability and validity of the NRM carried by individual subsamples that are normally in the form of discrete cubes (a typical volume is 7 cm^3) or U-channels that are typically 1–1.5 m long (Tauxe *et al.* 1983). A parameter commonly used to assess magnetic stability and accept or reject samples in a data set is the maximum angular deviation (MAD). With regards to subsamples of relatively wet sediments that cannot be thermally demagnetized, the MAD is obtained by principal component analysis (PCA) of alternating field (AF) demagnetization coercivity spectra, which is made to provide the inclination and declination of a Characteristic Remanent Magnetization (ChRM) (Kirschvink 1980) and identify (potential) multiple components of an NRM. There is, however, no defined threshold value of the MAD for ChRM acceptance or rejection, although 5° is often quoted (e.g. Barletta *et al.* 2010; Sagnotti *et al.* 2016). It must also be stressed that a low MAD does not necessarily mean that the underlying NRM directions represent the in-situ (post)-depositional magnetization, due to it primarily being a measure of equipment-specific analytical precision and the stability of the magnetic signal carrier. In other words, subsamples deformed by sampling can yield a seemingly acceptable MAD value, while any information about sampling induced deformation of the sediment fabric and, therefore, the primary magnetization remains concealed.

In a benchmark study, Marino & Ellwood (1978) advocated measuring the discrete-sample anisotropy of magnetic susceptibility (AMS) to detect deformed sediment fabrics that could lead to false palaeomagnetic conclusions. Reviews of the development of AMS as a petrophysical tool (e.g. Hrouda 1982; Tarling & Hrouda 1993; Parés 2015) illustrate the ability of this sensitive and non-destructive technique to identify natural and artificial deformations caused by physical stress. As pointed out by Rosenbaum *et al.* (2000) the inherently tedious, labor intensive, measurement of AMS (at the time of Marino & Ellwoods' 1978 study) restricted its use. Even today only a handful of sediment core-based palaeomagnetic studies have systematically utilized the method (e.g. Nowaczyk & Frederichs 1999; Rosenbaum *et al.* 2000; Nowaczyk 2003). Over the past decade or so, automated magnetic susceptibility bridges have been developed (e.g. Studýnka *et al.* 2014) and the effort required for a measurement has been significantly reduced, resulting in an increased number of studies that report AMS data. Novel applications include the reconstruction of palaeo-current directions, which has included fitting depth (∼time) averaged measurements of the ChRM declination according to a geo-axial dipole and subsequently rotating the AMS data (e.g. Tamaki *et al.* 2015; Sutereesak *et al.* 2017).

Our study was inspired by preliminary palaeomagnetic data obtained from three sites cored during IODP Expedition 347 *Baltic Sea Paleoenvironment* (Andrén *et al.* 2014, 2015) using a version of the IODP Advanced Piston Corer (APC) described by Jutzeler *et al.* (2014). Obrochta *et al.* (2017) used AMS data from one of these sites (M0063 located in the Landsort Deep; Expedition 347 Scientists 2015) to quantify sediment disturbance caused by degassing and expansion of organic-rich sediments upon recovery using the APC. Bowles (2006) also used AMS to demonstrate that drilling-induced deformation of carbonate-rich sediment recovered as part of ODP Leg 208 negatively affected the quality of palaeomagnetic data. Here, we present AMS and palaeomagnetic data obtained from two further IODP Expedition 347 sites (M0061 and M0062), which are located in the Ångermanälven estuary. The data from the IODP sites, where the aforementioned APC system was deployed, are subsequently compared to data obtained from a series of sediment cores that were later recovered from the same two locations using a Kullenberg piston corer (Kullenberg 1947). Systematic core splitting, subsampling methods and laboratory measurements were applied to both sets of subsamples. We suggest how stresses induced by coring (and sampling) are manifested in the AMS data. We subsequently develop a protocol that we use to accept or reject palaeomagnetic data according to (i) a combination of AMS parameters and a minimum inclination value predicted by time-varying geomagnetic field models and (ii) the statistical method of Deenen *et al.* (2011), which provides an A95 cone of confidence around virtual geomagnetic pole distributions.

2 SITE LOCATIONS, REGIONAL GEOLOGY AND STRATIGRAPHY

2.1 Site locations

The two IODP sites studied (M0061 and M0062) are respectively located in the outer and inner parts of the Ångermanälven River estuary, which is connected to the Bothnian Sea sector of the Baltic Sea (Fig. 1). Metamorphic rocks, such as gabbros, amphibolites and schists dominate the oldest unit in the area, which are related to the Svecofennian orogeny. Palaeoproterozoic rocks related to the Svecofennian orogeny also include granites, pegmatites and greywacke. The Quaternary (postglacial) geology of the northern Baltic Sea basin is dominated by tills and outwash deposits, glaciolacustrine rhythmites, debrites and a series of lacustrine clays and brackish-water mud drifts (Virtasalo *et al.* 2007).The area remains under the influence of glacial isostatic rebound and the current rate of land uplift is *ca*. 0.8 cm yr^{-1} (Ekman 1996). The highest postglacial shoreline in the area is approximately 286 m above sea level (Berglund 2004). Just after the regional deglaciation *ca*. 10.5 ka ago, the sites studied were located in a relatively open sea, but due to continued land uplift they are now located in an estuary (Hyttinen *et al.* 2016). Table 1 provides information about the site locations and more details can be found in Andrén *et al.* (2015). The Ångermanälven River estuary has been the focus of several studies of the regional Quaternary geology because of the formation of relatively thick sequences of varved clays and silts that provide a semi-continuous geochronology between the regional deglaciation at the end of the Weichselian glaciation and the present-day (Cato 1985).

2.2 Holocene sediment succession in Ångermanälven

Hyttinen *et al.* (2016) present a formal stratigraphic subdivision for the Holocene sediment succession in the Ångermanälven River estuary that is based on acoustic profiling and studies of the IODP Expedition 347 cores. This subdivision combines allostratigraphic and lithostratigraphic techniques (the CUAL approach as described by Räsänen *et al.* 2009) and we apply it to our study and use the same Lithological Units (LU) assigned by Hyttinen *et al.* (2016). The LUs were allocated depths according to the IODP Expedition 347 m composite depth (mcd) scale (Andrén *et al.* 2015).

Due to the 6 m recovery limit of the available Kullenberg piston corer (see Section 3), our study is limited to sediments that belong to the Hemsön Alloformation, which consists of brackish water muds composed predominantly of horizontal, planar, and parallel weakly laminated silty clay. The Hemsön Alloformation, which corresponds to LU3 described by Hyttinen *et al.* (2016) extends

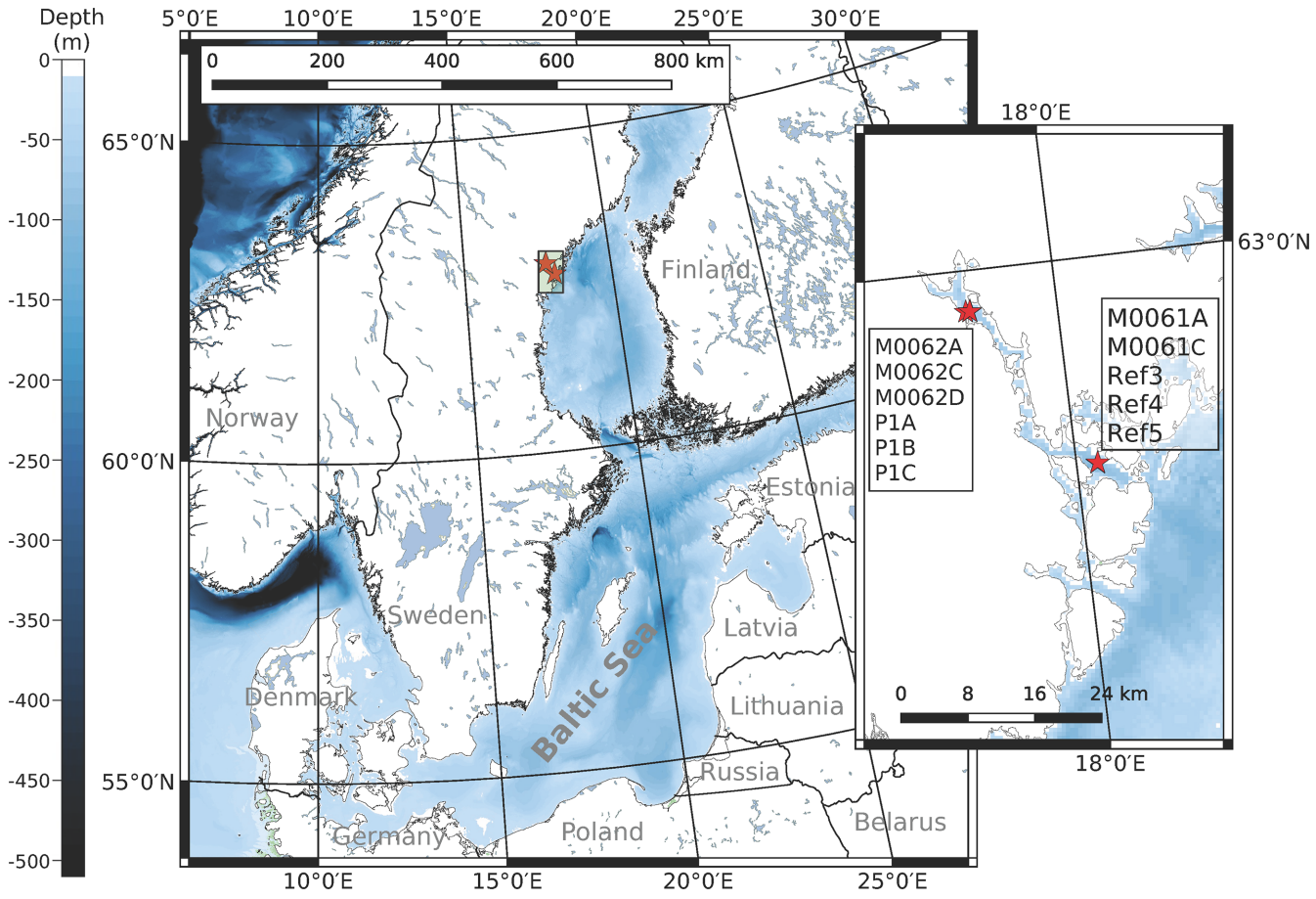

Figure 1. Overview of the Baltic Sea, the location of the Ångermanälven River estuary and the positions of IODP Sites M0061 and M0062.

Table 1. Summary of site locations and sediment cores used in this study.

Site name	Short name	Core sections	Latitude longitude (decimal degrees)	Elevation (m)	Corer type APC[3] KPC[4]	No. of discrete samples
M0061						
Hole-M0061A[1]	M0061A	2–1	62.77833, 18.04916	–87.9	APC	7
Hole-M0061C[1]	M0061C	1–1, 1–2,	62.77870, 18.04970	–87.9	APC	56
TRE-15-Ref001–03[2]	Ref3	1, 2, 3, 4	62.77864, 18.04975	–85.5	KPC	113
FIN-15-Ref001–04[2]	Ref4	1, 2, 3, 4	62.77864, 18.04975	–85.5	KPC	116
FIN-15-Ref001–05[2]	Ref5	1, 2, 3, 4	62.77864, 18.04975	–85.5	KPC	117
M0062						
Hole-M0062A[1]	M0062A	2–1, 2–2, 3–1, 3–2	62.95583, 17.79500	–69.3	APC	63
Hole-M0062C[1]	M0062C	1–1, 1–2	62.95571, 17.79530	–69.3	APC	46
Hole-M0062D[1]	M0062D	2–1, 2–2	62.95596, 17.79526	–69.3	APC	35
Fou-14–001-P1A[2]	P1A	1, 2, 3, 4	62.95577, 17.79456	–69.0	KPC	194
Fou-14–001-P1B[2]	P1B	1, 2, 3,4	62.95577, 17.79456	–69.0	KPC	190
TRE-15–001-P1C[2]	P1C	1, 2, 3, 4	62.95579, 17.79452	–69.0	KPC	166

[1]Integrated Ocean Drilling Program (IODP) site/hole identifier.
[2]Geological Survey of Sweden (SGU) site identifier.
[3]IODP hydraulic piston corer, or advanced piston corer (Andrén *et al.* 2015).
[4]Kullenberg piston corer (Kullenberg 1947).

to a maximum depth of 8.2 mcd at site M0061 and a maximum depth of 10.5 mcd at site M0062. LU3 at site M0061 is divided into two subunits, 61-LU3a (8.15–2.3 mcd) and 61-LU3b (2.3–0 mcd). LU3 at site M0062 has not been divided into subunits at this time. Palaeomagnetic samples from the upper part of 61-LU3a were weakly magnetized (<10 mAm^{-1}; Andrén *et al.* 2015) and we restrict this study to samples recovered from the top 3 mcd at site M0061, which includes the transition from 61-LU3a to 61-LU3b.

3 SAMPLING AND METHODS

3.1 Core recovery

The APC, which is a wireline hydraulic piston coring system, was used to recover cores from IODP sites M0061 and M0062 during the offshore phase of IODP Expedition 347 in late 2013 (Andrén *et al.* 2014). Three holes were cored at Site M0061 (M0061A-C) and four holes at Site M0062 (M0062-A-D). The sections relevant to our study are listed in Table 1.

A pertinent technical detail is that the APC cores were collected in successive 3 m sections (63 mm internal diameter) and no attempt was made to orient cores and subsequent core sections relative to an azimuth or to each other, but it is assumed that all sections were collected perpendicular to the mudline (i.e. vertical penetration). The core-barrel penetrated into the sediments when the hydraulic pressure above the fixed-piston caused brass pins to shear. This pressure was set to approximately 50 bar at Sites M0061 and M0062 (David Smith, personal communication, British Geological Survey) although the maximum pressure used during IODP Expedition 347 was 130 bar (Andrén *et al.* 2015). While no specific details are available about the penetration rate for any core section recovered, Jetzeler *et al.* (2014) mention a rate of 6–12 m s^{-1} for unconsolidated, water-saturated sediments. Thus, we estimate that each 3 m liner recovered by the APC was filled in approximately 0.5–0.25 s (recoveries at Sites M0061 and M0062 were almost 100 per cent).

A 6-m-long Kullenberg piston corer (forthwith referred to as KPC) was used to recover three cores at Sites M0061 (Ref3, Ref4 and Ref5) and M0062 (P1A, P1B and P1C) during field campaigns in 2014 and 2015 on board the Survey Vessel (SV) Ocean Surveyor, which is operated by the Geological Survey of Sweden (SGU). This cable operated piston corer can recover up to 6 m of sediments in a liner of 70-mm-internal diameter in a single stroke and it is designed not to exert pressure during impact, which could compress recovered sediments and potentially lead to oversampling. The SGU KPC system used had a mass of approximately 500 kg, of which 425 kg was the mass of lead weights positioned at the top of the 6-m-long barrel. An 'orange-peel' type core-catcher hindererd the loss of sediments during recovery (90 mm diameter). The core liners were marked during core recovery to ensure that each subsequently cut section had the same relative azimuth. To log the rate of penetration through the sediment package Star-Oddi™ magnetic sensors were attached to the upper part of the core barrel to log the time and depth. The sampling rate of the sensor was set to the highest possible frequency of 1 s. The logs of time and depth record when the trigger weight released and when the corer stopped penetrating sediment, and the results indicate that the KPC penetrated the sediments at a rate of 1 m s^{-1}, which is consistent with previous work estimating the speed of a KPC during freefall (e.g. Le Tirant 1979). The sensor data indicate that the corer did not decelerate during the penetration and the recovery was 100 per cent, but the low sampling frequency rate limits our understanding of the corer's behavior. The Star-Oddi™ sensors also recorded magnetic declination of the core barrel. No turning of the core barrel was detected by the sensors during deployments, but it was observed that some core liners had turned relative to the barrel's long axis. It is not known when this turning of the liners occurred and, therefore, no attempt was made to use the Star-Oddi™ sensor data to orient the palaeomagnetic declination data to a geographic azimuth. Details about each sediment core recovered are provided in Table 1.

3.2 Discrete sediment subsampling

The APC core sections were cut into nominal 1.5 m lengths and split along their lengths at the Bremen core repository (at the Center for Marine Environmental Science—MARUM) during the onshore phase of IODP Expedition 347. KPC core liners were cut into 1–1.5-m-long sections and split using a purpose built core-splitter owned by SGU or a Geotek core-splitter at the Department of Geological Sciences, Stockholm University. Common to all splitting procedures was that the wall of the liner was first cut with either an oscillating power tool or a sharp knife and a thin wire subsequently pulled through the core sections to provide two halves of sediment. Core section halves were then separated as carefully as possible before surface cleaning and description. Split APC core sections were imaged using a high-resolution line-scan camera attached to a Geotek Multi Sensor Core Logger (MSCL) prior to surface cleaning and description (Andrén *et al.* 2015) whereas lower-resolution line-scan images of a selection of archived KPC core sections from site M0062 were obtained using an Itrax core scanner at the Department of Geological Sciences, Stockholm University.

Standard sized plastic cubes with an internal volume of approximately 7.6 cm^3 (APC subsamples) or 7 cm^3 (KPC subsamples) were used to subsample all core sections within a few hours after splitting. We did not observe any inwards or outwards contraction of the split KPC liners prior to subsampling, which was observed by Shimono *et al.* (2014) to bias AMS data, but after several months the edges of the liners had contracted inwards by approximately 1 cm in total. Palaeomagnetic subsample cubes, with a hole in the base to let air escape, were gently pushed into the surface of each section core half and removed with non-magnetic tools. The APC core sections that contained units 61-LU3 and 62-LU3, and which were also part of the site's splice, were subsampled at 5 cm increments (Andrén *et al.* 2015), while the KPC core sections were subsampled at 3 cm increments. This sampling strategy resulted in a total of 1097 samples from the Hemsön Alloformation (the number of subsamples from each IODP hole and Kullenberg core site are listed in Table 1). After trimming and cleaning, lids were attached and the subsamples were wrapped, and stored in cool-rooms at 4 °C prior to palaeomagnetic and AMS measurements. Fig. 2 shows the orientation of the subsample boxes with respect to the split core liner and the protocols for reporting AMS directions and palaeomagnetic directions.

4 LABORATORY MEASUREMENTS

4.1 Anisotropy of magnetic susceptibility (AMS)

The AMS of each subsample was measured at Uppsala University, Department of Earth Sciences using an AGICO MFK1-FA magnetic susceptibility bridge in a field of 200 A m^{-1} operating at a frequency of 976 Hz. The bridge was calibrated with the manufacturers' standard and the results blank-corrected for the contribution of the instrument sample holder. A highly anisotropic standard made of thin steel wire was used to check that the specimen orientation parameters were entered correctly into the manufacturers' software and that the output data could be correctly compared with ChRM directions. The AMS method provides a second rank symmetric tensor, whose eigenvectors and eigenvalues are used to define a tri-axial ellipsoid with three principal magnetic susceptibility axes. The three magnetic susceptibility axes, which have specimen (instrument) directions that can be rotated to geographic coordinate system, are denoted as K_1 (maximum) $\geq$ K_2 (intermediate) $\geq$ K_3

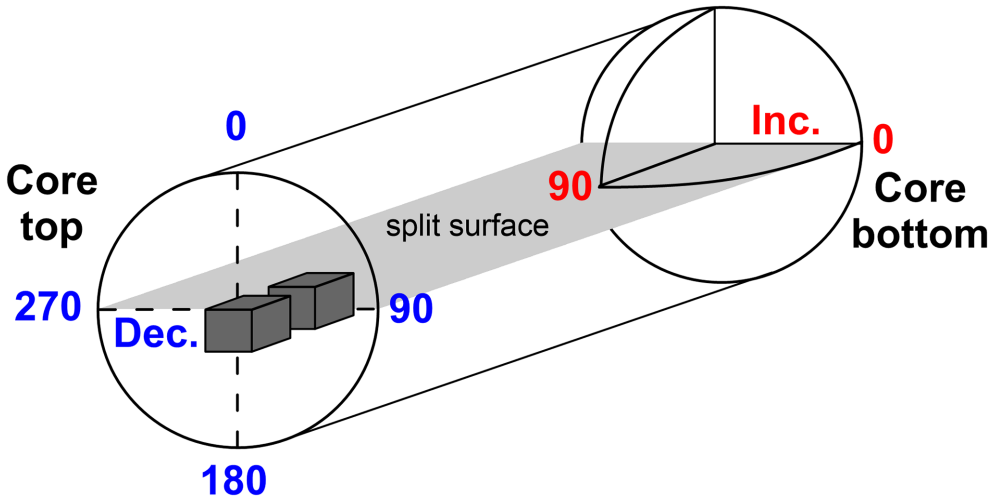

Figure 2. Illustration of the subsampling orientation with respect to the split-surface of a core section. Declination is determined by the analytical equipment used to measure anisotropy of magnetic susceptibility (AMS) and characteristic remanent magnetization (ChRM) and does not correspond to a geographic azimuth.

(minimum). AMS fabrics are commonly described in terms of the degree of the anisotropy (Pj) and the shape parameter (T), the latter of which ranges between oblate (+1) and prolate (–1). A low Pj is generally, but not exclusively, associated with unconsolidated sediments that have not been compacted, while a high Pj is found in compacted and layered sediments, which often have an oblate shape. Other terms can be used to describe the shape of the ellipsoid, such as lineation (L) and foliation (F). Hrouda (1982), Tarling & Hrouda (1993) and Parés (2015) provide reviews of the AMS method. In pristine sedimentary rocks, and varved sediments, one expects the directions of the K_1 and K_2 axes to be broadly distributed in the bedding plane unless strong bottom currents have biased the directions of elongated mineral particles. One also expects the minimum (K_3) axis to be perpendicular to the bedding plane, and the shape of the ellipsoid can be visualized as an oblate 'pancake' ($T \approx 1$). Deviations from these expectations, or biases to the core-specimen axes can indicate disturbances caused by sediment recovery or sampling techniques (e.g. Shimono *et al.* 2014). The wet mass of each subsample (corrected for the mass of the box and lid) was also obtained to two decimal places (in units of g) and used to calculate mass specific magnetic susceptibility (χ) normalized to wet mass.

4.2 Experimental test for field impressed AMS

For logistical reasons it was not possible to measure the AMS of the APC subsamples prior to AF demagnetization and the induction of artificial remanences, such as anhysteretic remanent magnetization (ARM) and isothermal remanent magnetization (IRM). ARM and saturation IRM (SIRM) data for all subsamples are not reported here, but it was necessary to rule out the possible influence of these magnetizations upon the AMS data, an influence that was reported as 'field-impressed magnetic anisotropy' by Potter & Stephenson (1990). In rocks where the low field magnetic susceptibility is dominated by paramagnetic and diamagnetic minerals the influence of field-impressed magnetic anisotropy on AMS is trivial, but it can become significant in rocks with relatively high concentrations of ferrimagnetic minerals (for example in the lavas measure by Potter & Stephenson 1990). To test for field impressed anisotropy of AMS we conducted an experiment on a suite of subsamples taken from two KPCs, P1A (n = 23) and P1C (n = 18) and measured the AMS before any alternating or direct fields were applied to them. The samples were then AF demagnetized according to the aforementioned procedure and exposed to a pulsed direct current (DC) magnetic field of 1 T (assumed to be an SIRM) along the stratigraphically vertical axis, and the AMS remeasured. The results of this test for field impressed anisotropy are shown in Fig. 3. As expected for unconsolidated sediments that are laminated and free of bioturbation the maximum (K_1) and intermediate (K_2) directions are distributed in the bedding plane, while the minimum axis (K_3) directions are perpendicular to the bedding plane. A few samples from P1A deviate from this ideal distribution, which will be explained further on, but the pre-SIRM and post-SIRM AMS measurements are not visually different. Thus, the test for field-impressed magnetic anisotropy in the sediments from the Hemsön Alloformation studied here is considered negative.

4.3 Palaeomagnetic measurements

All the IODP Expedition 347 APC subsamples were statically demagnetized along three-axes in a peak alternating field (AF) of 5 milliTesla (mT) and the magnetic remanence measured before and after this treatment during the onshore phase of the expedition at the Department of Geosciences (Marine Geophysics) at the University of Bremen. A 2G-Enterprises pass-through superconducting rock magnetometer (model SRM-4000) was used for these measurements. The IODP APC subsamples were then transported to Lund University for more detailed analyses that were also applied to the KPC subsamples. Using a 2G-Enterprises pass-through SRM-760 all the subsamples were stepwise demagnetized at fields of 0, 5, 10, 15, 20, 30, 40, 60 and 80 mT and the remanent magnetization recorded after each demagnetization step (10 samples from P1B were removed from the palaeomagnetic data set due to faulty AF demagnetization). The ChRM of each subsample, related to the magnetometer axes, was obtained using PCA analysis according to the method outlined by Kirschvink (1980) by using an unpublished MatLab script written by B. Lougheed ('EasyZijder') with the ChRM based on the data obtained from AF steps 10–60 mT. The average ChRM declination for each KPC core was calculated and then rotated to zero so that the KPC declination results are henceforth shown as deviations around 0°. This rotation was not

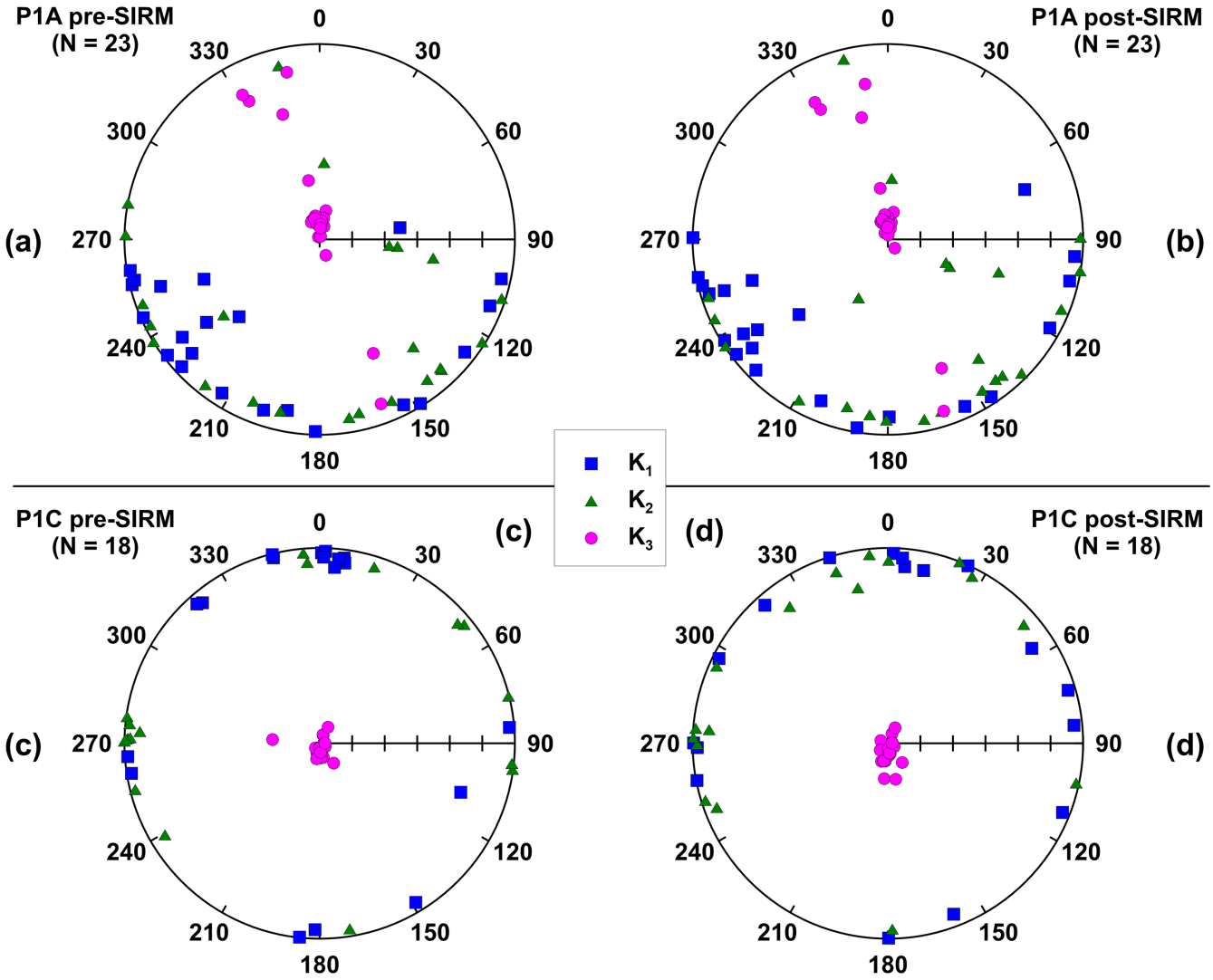

Figure 3. Results of a test for field-impressed AMS. The left-hand side lower hemisphere, equal area projections (a and c) show the directions of the three principal AMS axes (K_1, K_2 and K_3) of subsamples taken from the Hemsön alloformation (cores P1A and P1C) before induction of an SIRM at 1T. The right-hand side projections (b and d) show the directions of the three axes after the acquisition an SIRM at 1T. There is no significant difference in the distributions and the test is negative.

possible for the ChRM declinations obtained from the APC cores because successive core-sections were not oriented with respect to a common azimuth (Section 3.1).

5 RESULTS

5.1 Principal AMS axes

Fig. 4 shows the specimen directions of the three principal AMS axes for all samples from the two key IODP sites, divided into cores collected by the APC and the KPC. The mean directions and 95 per cent confidence limits for each set of subsamples are provided in Table 2. As predicted for horizontally bedded sediments, the vast majority of the K_1 and K_2 axes have inclinations close to 0 degrees, with the exception of some samples from P1A and P1B, in which the K_1 and K_2 directions trend towards the vertical and the K_3 axis shallows. The declinations of the K_1 axis of the subsamples taken from APC core sections (M0061 and M0062) are distinctly and tightly grouped within the 90–270 degree specimen axis, which is the direction across the split cores' surfaces (not the 'push' direction of the subsampling boxes). In contrast, the declinations of the K_1 and K_2 directions of the vast majority of the subsamples taken from the KPC liners (Ref3, Ref4 and Ref5; P1A, P1B and P1C) have a wider distribution around the horizontal (bedding plane) and show no preferred alignment to a specimen axis.

5.2 AMS ellipsoids and shape parameters

Fig. 5 illustrates the relationship between Pj and T for all the subsamples from the Hemsön Alloformation according to location and type of corer used. The vast majority of subsamples from site M0061 (Figs 5a and c) have oblate ellipsoids with a relatively high Pj, while the complete data set shows a positive curvilinear relationship, whereby samples with a low Pj possess a prolate fabric. The set of subsamples from site M0062 (Figs 5b and d) shows the same general trend, but also contain samples that deviate from a curvilinear trend and have a prolate fabric with a high Pj. It is noteworthy that the set of subsamples recovered from M0062 with the APC

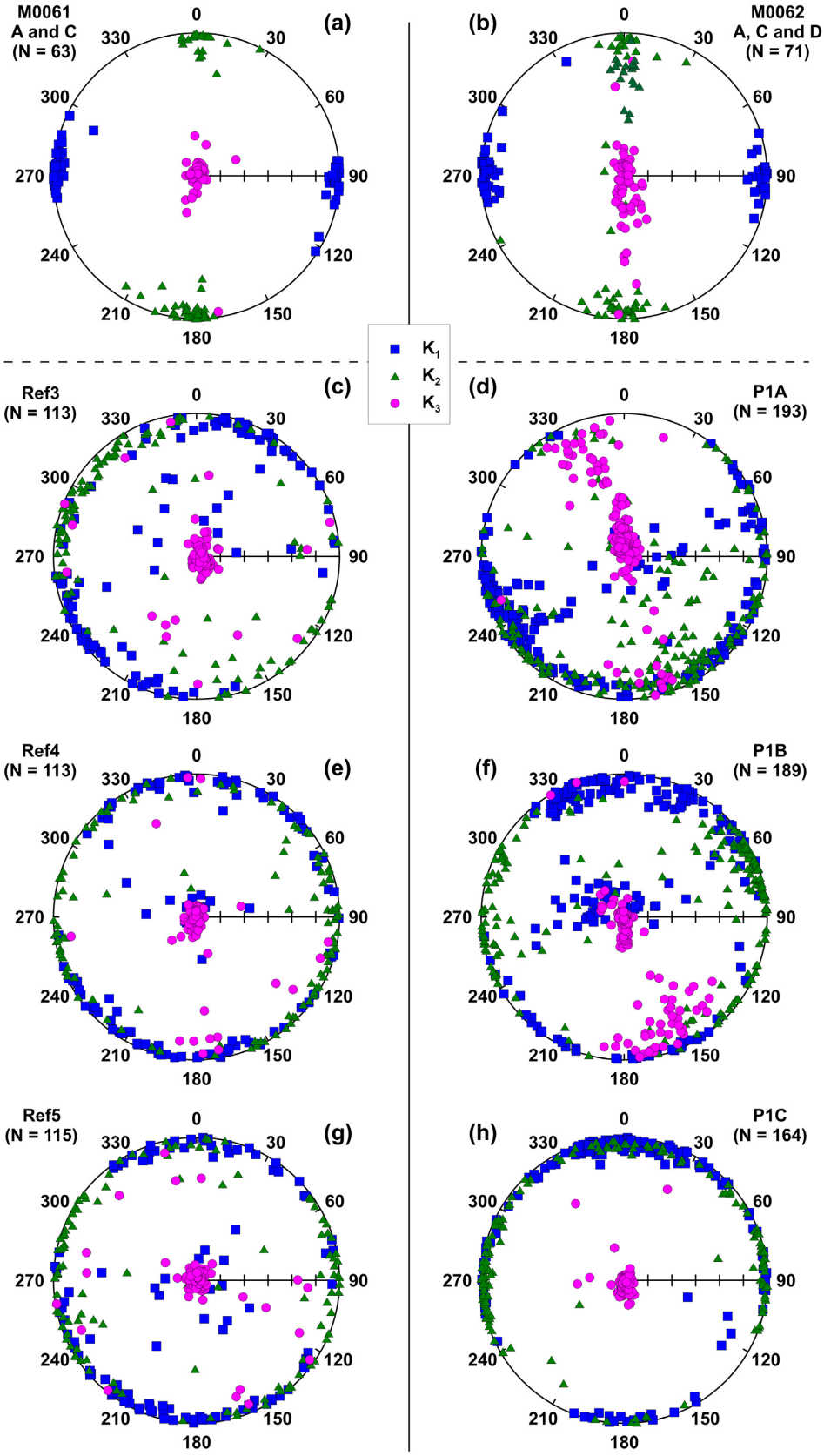

Figure 4. Lower hemisphere, equal area projections that show the directions of the three principal AMS axes of all subsamples on a core/hole basis. The statistics are listed in Table 2. Data obtained from the APC sections (a and b) are biased along the sample axes, with the K_1 direction across the surface of the split core. The distribution of the AMS axes for KPC sections (c–h) show no such bias and conform to a fabric expected for horizontally bedded sediments, with the exception of some samples in which the K_1 trends towards the vertical (poles).

Table 2. AMS statistics.

Hole/core name(s)	AMS axis	Inclination (°)	Declination (°)	Tensor
M0061 (A,C)	K1	0.5 ± 2.8	272.4 ± 7.5	1.014
	K2	0.9 ± 3.8	182.4 ± 7.5	1.005
	K3	89.0 ± 2.8	34.7 ± 3.9	0.980
Ref3	K1	1.5 ± 4.8	226.9 ± 36.0	1.012
	K2	3.1 ± 6.3	317.0 ± 36.1	1.010
	K3	86.6 ± 3.8	110.8 ± 7.4	0.978
Ref4	K1	0.0 ± 4.8	22.9 ± 56.5	1.011
	K2	0.3 ± 3.9	112.9 ± 56.5	1.010
	K3	89.7 ± 3.7	291.9 ± 5.0	0.979
Ref5	K1	0.9 ± 4.4	194.9 ± 46.2	1.011
	K2	0.5 ± 4.6	284.9 ± 46.2	1.009
	K3	89.0 ± 4.4	42.4 ± 4.6	0.980
M0062 (A, C, D)	K1	1.5 ± 4.3	269.8 ± 5.9	1.022
	K2	5.1 ± 5.6	360.0 ± 15.1	1.002
	K3	84.7 ± 4.5	163.6 ± 15.2	0.976
P1A	K1	1.8 ± 6.2	250.7 ± 19.8	1.011
	K2	10.7 ± 17.6	160.4 ± 20.2	1.004
	K3	79.1 ± 6.2	350.0 ± 18.1	0.985
P1B	K1	2.2 ± 6.9	60.0 ± 45.5	1.010
	K2	6.9 ± 13.1	329.7 ± 45.8	1.008
	K3	82.8 ± 6.6	167.9 ± 82.8	0.982
P1C	K1	2.7 ± 3.1	354.1 ± 48.7	1.020
	K2	0.1 ± 2.2	264.1 ± 48.7	1.018
	K3	87.3 ± 2.3	172.8 ± 3.2	0.962

(Fig. 5b) do not follow the curvilinear relationship. The highest degrees of anisotropy are found in a few samples that have a prolate shape and were taken with the KPC (Fig. 5d). Another illustration of the AMS data is provided in Fig. 6, where the angular difference between the expected K_3 axis for perfectly horizontal bedding (90° with respect to Earth's surface in this case) and the measured K_3 angle of each subsample (denoted as 90-K_3) is shown. Hrouda & Kahan (1991) argued that an angular difference greater than 15° suggested significant deviation from horizontal bedding. This value was applied by Suteerasak *et al.* (2017) to identify sections of sediments recovered from the Bothnian Bay that had been deformed by gravity coring. As shown in Fig. 6, a large number of subsamples recovered from both sites by the KPC corer can be identified as deformed, while the deformation caused by the IOPD-APC is most significant at site M0062.

5.3 Stratigraphic (depth) trends in AMS and palaeomagnetic data

Fig. 7 (M0061) and Fig. 8 (M0062) show the ChRM directions, χ, MAD values, degree of AMS (Pj), the 90-K_3 inclination parameter and the NRM intensity (J) against sediment depth. The ChRM inclination scale includes the GAD predicted inclination and the lower limit of inclination (65°) predicted by time-varying geomagnetic field models for the last 6000 yr at the site location (Nilsson *et al.* 2014; Panovska *et al.* 2015).

With regards to site M0061 the most important features of the data shown in Fig. 7 are as follows: (i) inclination varies around the predicted GAD, although some subsamples taken from the KPC (Ref3, Ref4 and Ref5 plot below the models' predicted minimum of 65° and the inclinations of nearly all the subsamples from APC cores (Holes M0061A and M0061C) are steeper than the GAD prediction; (ii) the majority of subsamples have MADs lower than 5°, although there are some higher values at the top and bottom of the cores, which have weaker NRM intensity; (iii) 90-K_3 values are steeper than 15° in the upper 1 m of the three KPCs (and the upper 0.5 m of the sequence recovered by the APC). In general, these steep 90-K_3 values are associated with a lower degree of anisotropy (Pj) and (iv) the downcore trends in ChRM inclination and NRM intensity are similar, while the ChRM declination trends are difficult to compare due to the absence of orientation between successive IODP core sections. We note an unexplained, systematic difference between the χ of subsamples measured during the IODP Expedition 347 Onshore Science Party and those measured in Uppsala, but there is not much downcore variation.

With regards to site M0062 the most important features of the data shown in Fig. 8 are as follows: (i) many ChRM inclination values obtained for APC subsamples in Holes M0062A (0–1 mcd) and M0062D (3–4.5 mcd) are much lower than the modelled minimum of 65° for the past 6000 yr, which also applies to subsamples from the upper meter of Kullenberg core P1A; (ii) subsamples from the top 0.5 m of the cores (when taken) have MAD values that exceed 5°; (iii) the 90-K_3 values approach the maximum possible (90°) in the upper 1–2 m of KPCs P1A and P1B, and there are large angular differences in the IODP samples from Hole 62D; (iv) it is noteworthy that the high 90-K_3 values are associated with low NRM intensity and (iv) the depth trends in ChRM inclination and declination are quite similar between cores, with the exceptions of sections of individual cores that have high 90-K_3 values. We note that two peaks in ChRM inclination exist in the three KPCs (P1A, P1B and P1C) at depths of approximately 5.5 and 4 m. In general, Pj trends upwards towards lower values, except in the top 0.5 m of KPCs P1A and P1B, where it rises to >1.1, and these samples have prolate AMS ellipsoids (Fig. 5d).

The ChRM directions for each hole/core are also shown as lower hemisphere equal area projections in Fig. 9, which illustrate the distributions of data points that have inclinations shallower than the model predictions for the past 6000 yr. The sample sets recovered from site M0062 (IODP Holes C and D and KPC P1A and P1B) contain numerous samples that have inclinations lower than the predicted minimum of 65°.

To further assess the statistical quality of the palaeomagnetic directions in terms of PSV we applied the Fisher (1953) based method of Deenen *et al.* (2011) to the KPC subsample sets (we did not apply this method to the APC data because the core sections were not oriented to a common azimuth). As recommended by Deenen *et al.* (2011) the ChRM obtained for each subsample (dispersed around the respective core declination average) was converted to a virtual geomagnetic pole (VGP) and the VGPs compiled for each site. The *Paleomagnetism.org* platform provided by Koymans *et al.* (2016) was used for an analysis in which a variable Vandamme (1994) cut-off was applied to accept or reject data. The analysis (summarized in Table 3) led to the rejection of 21 data points from the compiled KPC data set from site M0061 (320 of 341 accepted) and 27 data points from the KPC data set from site M0062 (510 of 537 accepted). The accepted data points provide, for both data sets, A95 values that fall within or on the edge of the A95min and A95max reliability envelope (Deenen *et al.* 2011). These dispersions would be considered statistically reliable in terms of establishing a VGP (Deenen *et al.* 2011) and in the following discussion we compare the results of the statistical analysis to filtering according to AMS-based 90-K_3 parameter and the predicted inclination minimum.

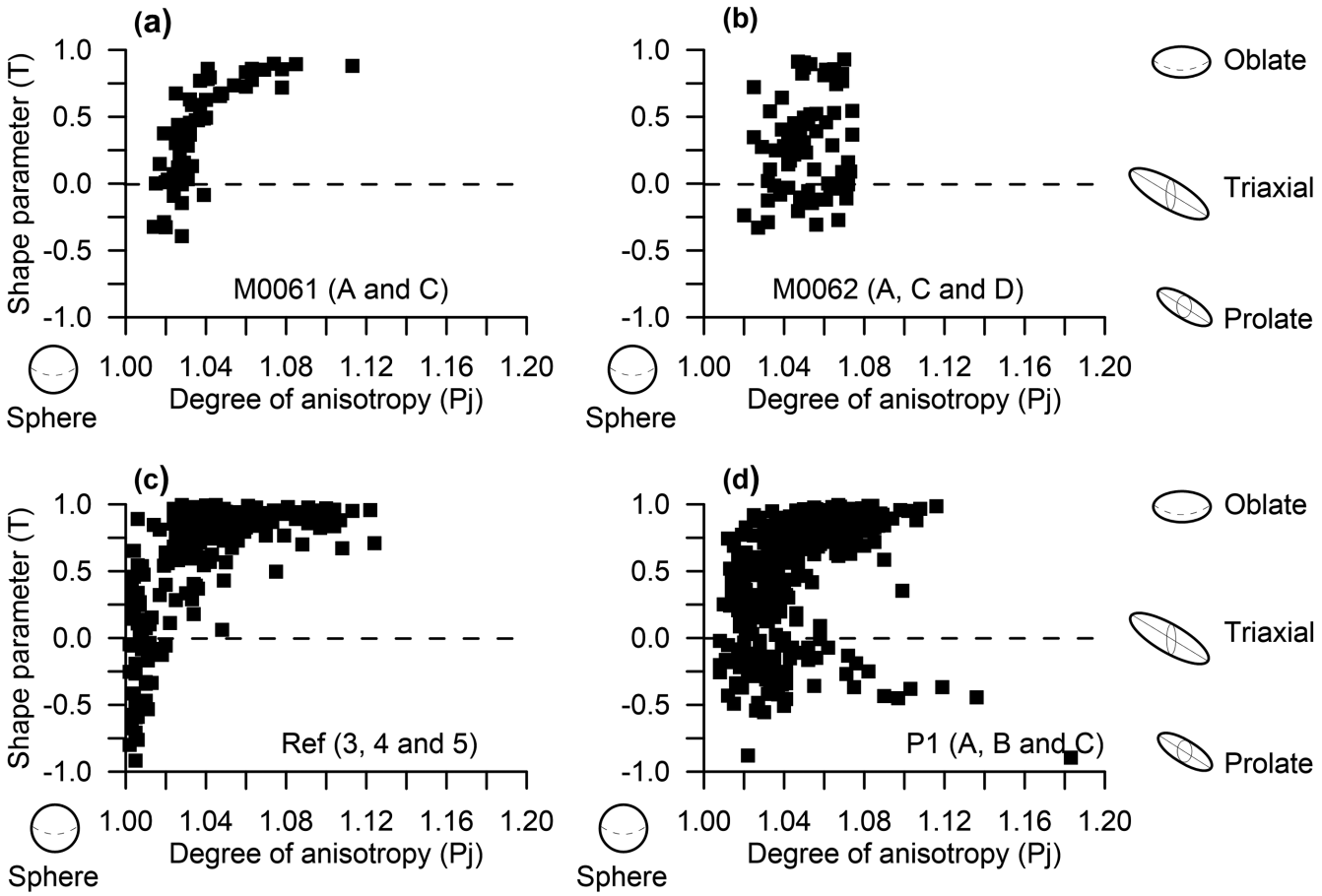

Figure 5. Illustrations of relationship between the degree of anisotropy (Pj) and the shape parameter (T). Subsamples from cores taken at site M0061 (a and c) show a typical curvilinear relationship with increasing anisotropy and more oblate ('pancake') fabrics. Many subsamples from site M0062 (b and d) do not follow the general trend and some taken with the KPC have prolate fabrics and a relatively high degree of anisotropy (d).

6 DISCUSSION

6.1 Possible causes of systematically biased principal AMS axes in sediments

Detailed, systematic AMS studies of Rosenbaum *et al.* (2000) found that artificial AMS fabrics in drill cores had been caused by core deformation and that palaeomagnetic data associated with previously undetected deformations had been incorrectly interpreted as geomagnetic excursions, a potential problem that Bowles (2006) raised with regards to drilled sediment cores recovered during ODP Leg 208. Széréméta *et al.* (2004) used AMS to demonstrate that the top 15–18 m of sediment had been oversampled by the Calypso piston corer regularly used on the research vessel *Marion Dufresne*. In a comparative AMS study of different coring techniques applied to soft sediment cores Shimono *et al.* (2014) showed that cores taken from the same site had different AMS fabrics according to the type of liner used, rather than the type of corer (gravity core and piston core). They argued that dissimilarities in the deformation (inward contraction or outwards expansion) of the core liners that took place after core-splitting and prior to subsampling were responsible for stresses imposed across the (horizontal) bedding plane. However, they argued that the palaeomagnetic directions were not affected because the inclination average was close to that predicted by a GAD. Earlier studies, such as that by Gravenor *et al.* (1984) have also considered the subsampling effect (the subsample cube 'push direction') on AMS directions and on palaeomagnetic data.

Our combined AMS and palaeomagnetic study of discrete subsamples taken with the APC at Sites M0061 and M0062 show the same coincidence between the three principal AMS axes and the subsample axes that Obrochta *et al.* (2017) noted for subsamples taken at the Landsort Deep Site M0063 using the same APC. Due to the lack of a similar systematic bias of the AMS axes directions in subsamples taken from the KPC sections, which were taken in precisely the same way as the subsamples from the APC core sections, we can rule out any bias caused by pushing of the subsampling boxes into these sediment (e.g. Gravenor *et al.* 1984).

Obrochta *et al.* (2017) and this study show that the K_1 declinations are concentrated along the axis parallel to the split core surface, which Copons *et al.* (1997) and Shimono *et al.* (2014) credited to the outwards expansion of the core liner after splitting (and prior to subsampling). With the technical information available we are not able to conclude that the APC core liners used in Expedition 347 expanded outwards during (and/or after) core splitting because of liner relaxation, except state that this process cannot be ruled out and could be responsible for the results. A second possibility, is that some core-splitters apply force from above and below the liner during splitting to prevent movement and loss of sediment while the sides are cut, which could produce an eccentric (oval) shape and potentially a similar effect on AMS tensors as the core liner is compressed. A third possibility, as raised by Shimono *et al.* (2014)

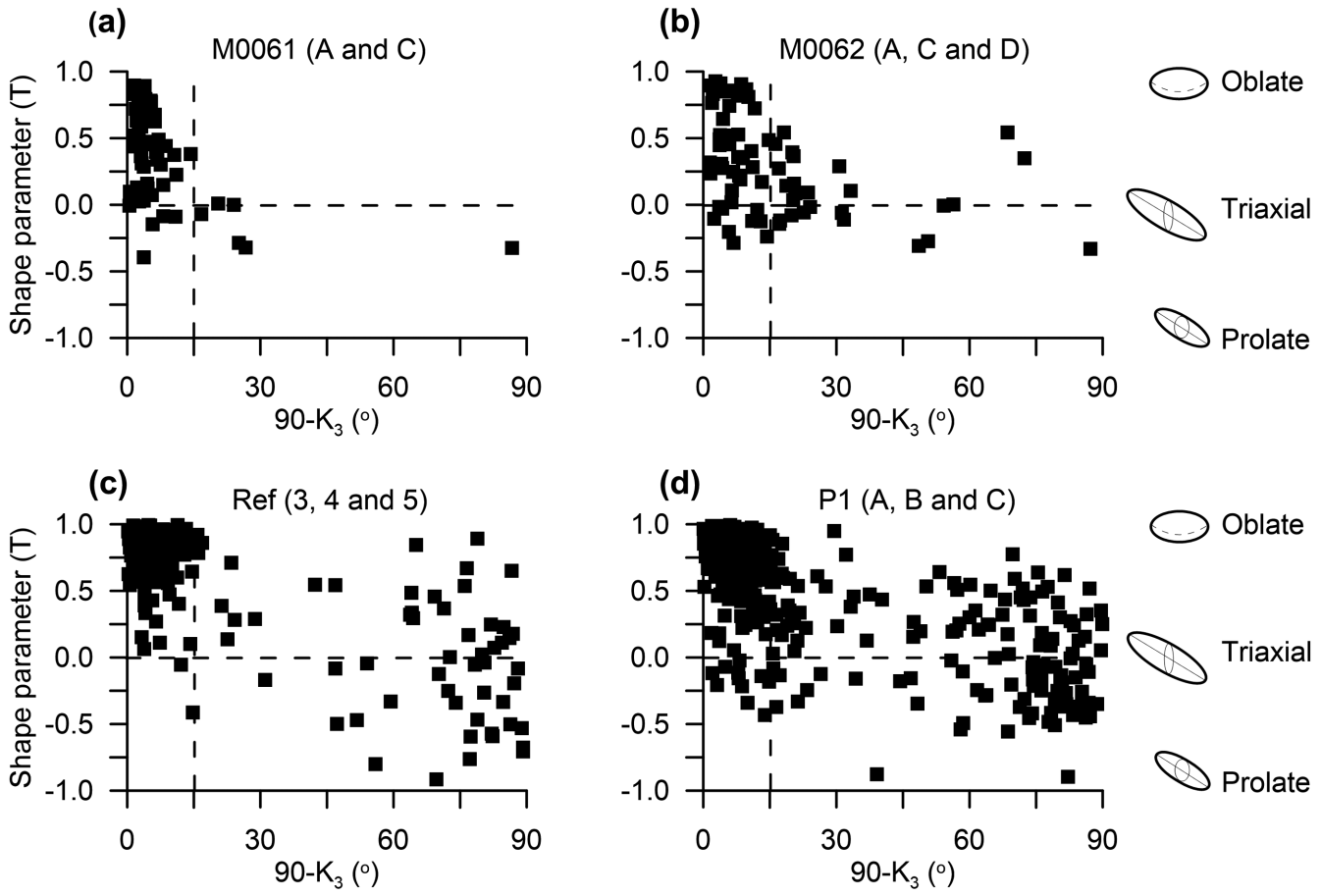

Figure 6. The difference between the expected inclination of the minimum AMS axis (K_3) for horizontally bedded sediments (90-K_3) and the shape parameter (T) for subsamples taken with the APC (a and b) and the Kullenberg corer (c and d). A 90-K_3 value of >15° has been suggested as indicative of disturbed sediment. While most data points have horizontal, oblate fabrics many samples taken with the KPC have triaxial to prolate shapes that are characterized by high 90-K_3 values.

is that pressure caused by dragging a tool (a scraper) parallel to the (horizontal) bedding plane, to clean the surface, might create the same result.

A difference between the APC deployments in the Landsort Deep site (451 m water depth) and those from the Ångermanälven estuary (water depth of 86 m at Site M0062 and 68 m at Site M0062) is that only 1.5–2 m long APC drives were used at the former site, which allowed the gas-rich sediment to expand upwards into the standard ∼3 m long liners upon decompression. This expansion, which was most obvious in the upper 0.7 m of each 3 m liner, caused the K_1 to reach almost 90° (roughly equivalent to a 90-K_3 value of 90°). Such unusual sediment expansion (causing recovery of up to 200 per cent) was not encountered during IODP Expedition 347 operations at Sites M0061 and M0062 and standard 3 m drives into ∼3 m liners were employed. Unfortunately, because line-scan images of the split IODP core sections were take prior to surface-cleaning and that only lower resolution images of the split KPC sections were obtained, systematic visual evidence of sediment disturbance is not as clear as it could be. However, Fig. 10 shows three examples of the type of sediment structure obtained for 0.5 m thick sections of sediment recovered from site M0062. For example, the sediment between 3.76 and 4.26 mcd has been radially deformed by the IODP-APC and is characterized by relatively high 90-K_3 values and low ChRM inclination values (Fig. 8), which are similar to the results obtained by Bowles (2006). The equivalent section obtained by the KPC retains horizontal bedding and a horizontal, oblate AMS ellipsoid but, on the other hand, sediment between 1.75 and 1.25 mcd in the same core shows clear indication of vertical 'stretching' (note that the photograph is of an archived half and some sediment was lost from this half during the splitting process), which is also identified in the AMS data by 90-K_3 values close to 90° (Fig. 8).

The AMS data sets obtained from the KPC sections show sampling induced deformation that is confined to the upper sections and is characterized by K_1 directions that approach the vertical (90°), similarly high 90-K_3 values and prolate AMS ellipsoids. We consider the cause of this deformation to be under-sampling during the initial stages of recovery. This effect is most obvious in cores from M0062 (P1A, P1B) and extends down to a sediment depth of 2 m, while the influence is restricted to the upper 0.5 m in the three KPCs from Site M0061. We emphasize that high 90-K_3 values (>15°) are often, but not exclusively, associated with AMS shape factors that trend towards prolate and lower NRM intensity, which collectively indicate vertical 'stretching' of the sediment. Detailed mineral (rock) magnetic data (not presented in this paper) indicate that the ferromagnetic mineral assemblage of the Hemsö formation is dominated by pseudo-single domain and multi-domain (titano-)

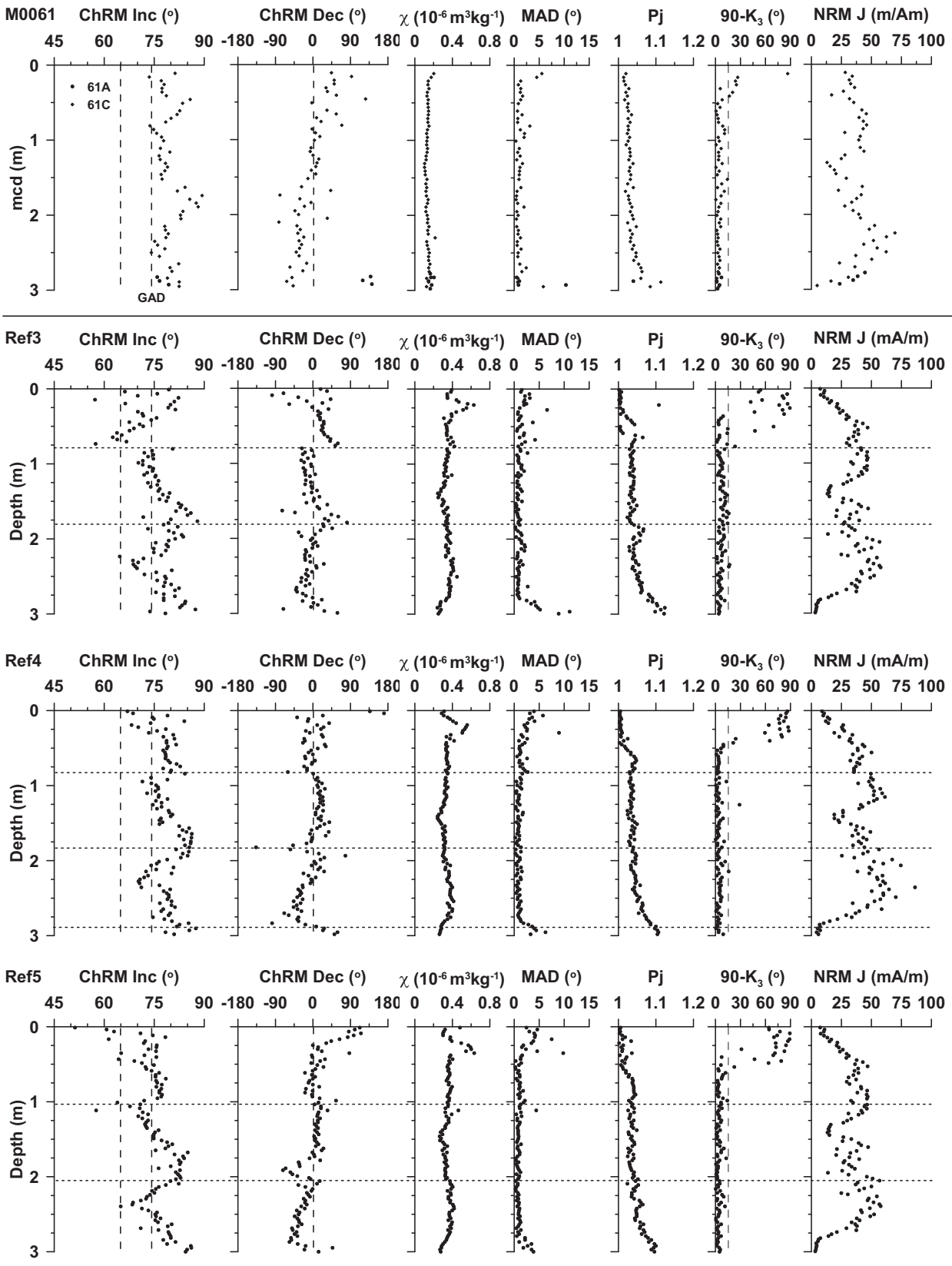

Figure 7. ChRM directions, wet-mass normalized magnetic susceptibility (χ), maximum angle of deviation (MAD) obtained from the ChRM analyses, the degree of anisotropy (Pj), the 90-K_3 inclination parameter and the intensity of the NRM (J) for all core sections analysed from IODP site M0061 plotted against depth in the sediment. The upper row of plots are the spliced data from the IODP holes. The site GAD inclination prediction of 74°, the minimum inclination predicted by time varying geomagnetic field models for the past 6000 yr (65°) at the site, and the 90-K_3 threshold angle of 15° are indicated by vertical dashed lines. Horizontal dashed lines show core-section breaks.

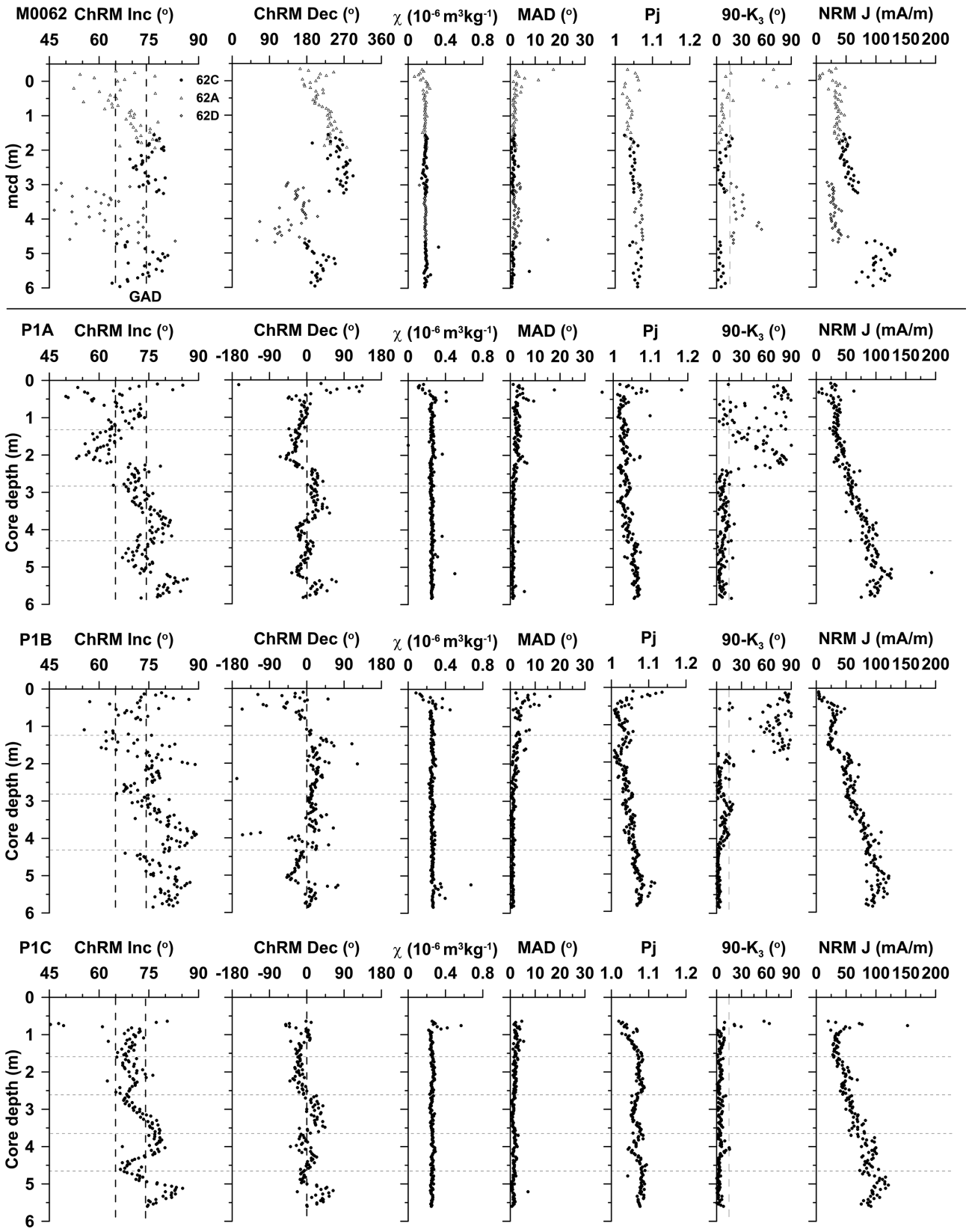

Figure 8. ChRM directions, wet-mass normalized magnetic susceptibility (χ), maximum angle of deviation (MAD) obtained from the ChRM analyses, the degree of anisotropy (Pj), the 90-K_3 inclination parameter and the intensity of the NRM (J) for all core sections analysed from IODP site M0062 plotted against depth in the sediment. The upper row of plots are the spliced data from the IODP holes. The site GAD inclination prediction of 74°, the minimum inclination predicted by time varying geomagnetic field models for the past 6000 yr (65°) at the site and the 90-K_3 threshold angle of 15° are indicated by vertical dashed lines. Horizontal dashed lines show core-section breaks.

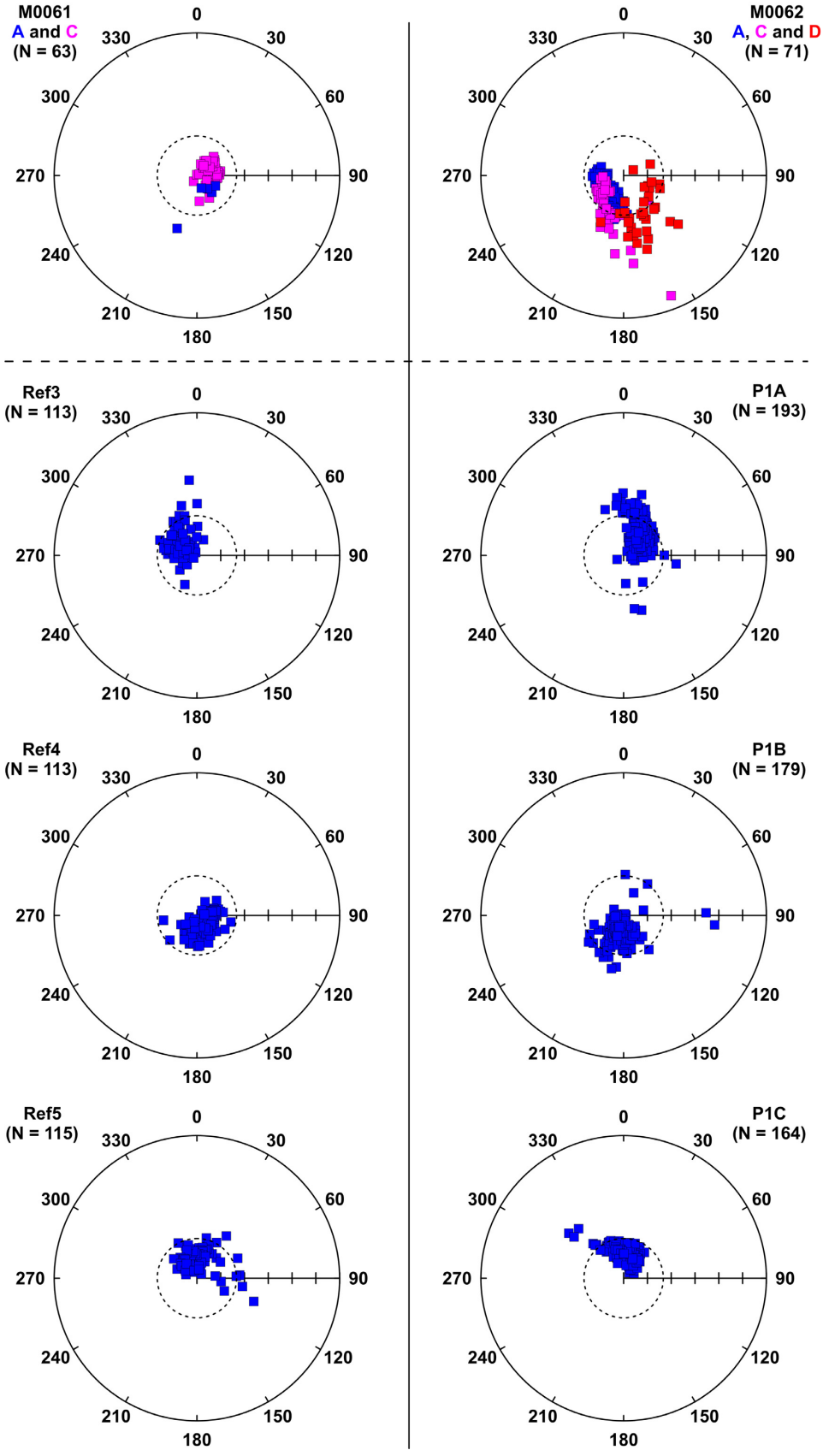

Figure 9. Lower hemisphere, equal area projections that show the ChRM directions of all subsamples on a core/hole basis, with M0061 to the left and M0062 to the right. The uppermost projections shows the data from the IODP-APC while the lower rows show data from the Kullenberg cores. The circular dashed line in each plot indicates the minimum inclination predicted by time varying geomagnetic field models for the past 6000 yr (65°).

Table 3. Summary of palaeomagnetic statistics undertaken on KPC data sets from IODP sites M0061 and M0062 according to the method of Deenen *et al.* (2011) with a variable Vandamme (1994) cut-off.

Site name Core name	Ns	$N_{accepted}$ -N	$\bar{x}$ Inc. (°)	A95	A95min	A95max
M0061						
Ref3, 4 and 5	341	-21	78.2	1.2	1.2	2.2
M0062						
P1A, B and C	537	-27	74.9	1.1	1.0	1.6

Figure 10. Line scan images of 0.5-m-thick sediment sections (4.26–3.76 mcd) from M0062 Hole D (left) and its equivalent section in the KPC core P1A (middle) and a section equivalent to a mcd of 1.75–2.25 in a higher section in P1. The left image illustrates the disturbance of the sediment structure caused by sampling with the APC. The sediment at this depth that was recovered by the KPC (middle) retained horizontal bedding. The sediment section to the right appears 'stretched' but does not have the conical structure characteristic of many sections of cores taken with the APC.

magnetite, so we rule out the possibility that the steep 90-K_3 angles are the result of an inverse AMS fabric due to single-domain magnetite effects (Potter & Stephenson 1988; Parés 2015). The AMS data set obtained from the KPC is free of the bias of AMS K_1 axis across the split core surfaces that characterizes the data from the APC. Some sections of sediment recovered by the APC show a conical structure, probably caused by frictional dragging down of the sediment in contact with the inside of the core-liner (Bowles 2006).

6.2 Acceptance of palaeomagnetic data using AMS data, modelled inclination and Fisher statistics

When the principal AMS axes are systematically biased into directions associated with sampling (corer penetration and recovery) and subsampling (core splitting, cleaning and pushing of sample boxes into the sediment) it is important to assess the potential effect on palaeomagnetic vector data. Clearly, it is critical to identify (sub-)sampling induced bias on the principal AMS axes if they are used to reconstruct palaeocurrent directions, especially if palaeomagnetic data are used to orient the cores to an azimuth.

Deformation induced by the different sampling methods appears to have contributed to scattered data and uncertainty in the palaeomagnetic data sets based on subsamples taken from the APC and KPC. The main reason for applying palaeomagnetic methods to the sites visited by IODP Expedition 347 was to potentially transfer ages from a regional PSV master curve (FENNOSTACK; Snowball *et al.* 2007) by identifying similar patterns in inclination and declination, possibly complemented by comparison to predictions of time-varying geomagnetic field models. In this study we are able to compare the ChRM inclinations to predictions based on a time-varying geomagnetic field model, which is constrained by archaeomagnetic and sedimentary data, and make a statistical assessment of the ChRM directions as described in section 5.3. We choose to use a 90-K_3 value of 15° and a model predicted inclination minimum of 65° to accept or reject data, which is illustrated in Fig. 11 and a summary is shown in Table 4. VGP data points accepted by the method of Deenen *et al.* (2011), as described in section 5.3, were rotated back to ChRM directions. The results of these filtering steps are summarized in Fig. 12, which illustrates the initial data sets, the data points rejected by each method (including data points rejected by both methods) and data points that pass all our criteria. Perhaps the most important result illustrated in Fig. 12 is that the statistical method does not reject samples that have relatively steep inclinations, but that were rejected by the application of the 90-K_3 threshold of 15°. In Fig. 13 we show preliminary stacks of the accepted ChRM inclination data obtained for the suite of Kullenberg cores at both IODP sites, alongside the prediction of Nilsson *et al.*'s (2014) pfmk9.1b model and the relative inclination from FENNOSTACK (Snowball *et al.* 2007). A radiocarbon-based age model for site M0061 was published by Dijkstra *et al.* (2018) and interpolated ages at 0.5 m increments (Warnock *et al.* 2017) are shown in Fig. 13. The regional peak in the abundance of *Picea* pollen dated to ca. 2200 Cal. BP, which was identified in M0061 at 2.6 mcd and in M0062 at 4.6 mcd by Warnock *et al.* (2017), lies just below a distinct unit of low inclinations that can correspond to the FENNOSTACK inclination feature δ, identified and dated to 1840 Cal. BP (Snowball *et al.* 2007). Warnock *et al.* (2017) correlated diatom data between sites M0061 and M0062 and tentatively transferred an age of 4000 Cal. BP to the first occurrence of *Picea* pollen at a depth of 5.5 mcd in site M0062. However, as discussed by Warnock *et al.* (2017) alternative ages of the first occurrence

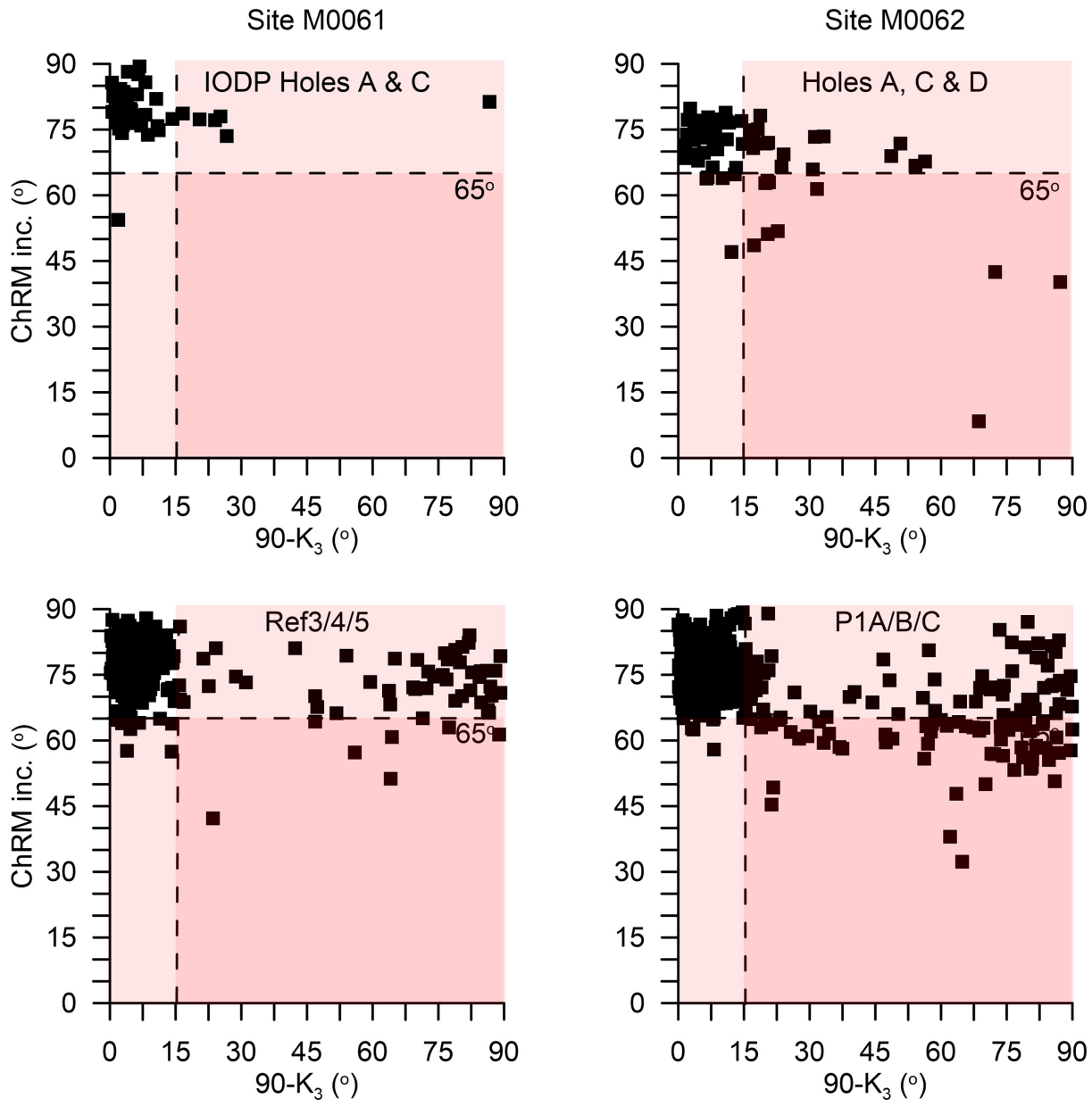

Figure 11. The 90-K_3 values versus the ChRM inclination for all samples based on core sites (M0061 to the left and M0062 to the right) and corer type (APC upper row, KPC lower row). The coloured panels indicate samples that should be rejected as valid palaeomagnetic data based on either too high (>15°) 90-K_3 values (bottom left in each plot), inclinations lower than model predictions (top right in each plot), or both criteria (bottom right in each plot). Data that plot in the top-left corner of each plot can be accepted as viable palaeomagnetic data.

Table 4. Summary statistics of inclination data from Kullenberg core subsamples before and after acceptance according to ChRM inclination >65° and 90-K_3 <15°.

		Primary data		Accepted data		
Site name	Short name	ChRM Inc. $\bar{x}$	ChRM Inc. 95%	ChRM Inc. $\bar{x}$	ChRM Inc. 95%	$n_{filtered}$-n
M0061						
TRE-15-Ref001–03	Ref3	75.44	1.50	76.83	1.10	-11
FIN-15-Ref001–04	Ref4	78.53	1.04	79.15	0.80	-10
FIN-15-Ref001–05	Ref5	75.28	1.61	76.40	0.84	-10
M0062						
Fou-14–001-P1A	P1A	70.83	1.69	74.66	0.99	-70
Fou-14–001-P1B	P1B	76.22	1.76	77.73	1.25	-39
TRE-15–001-P1C	P1C	72.11	1.26	72.64	0.70	-9

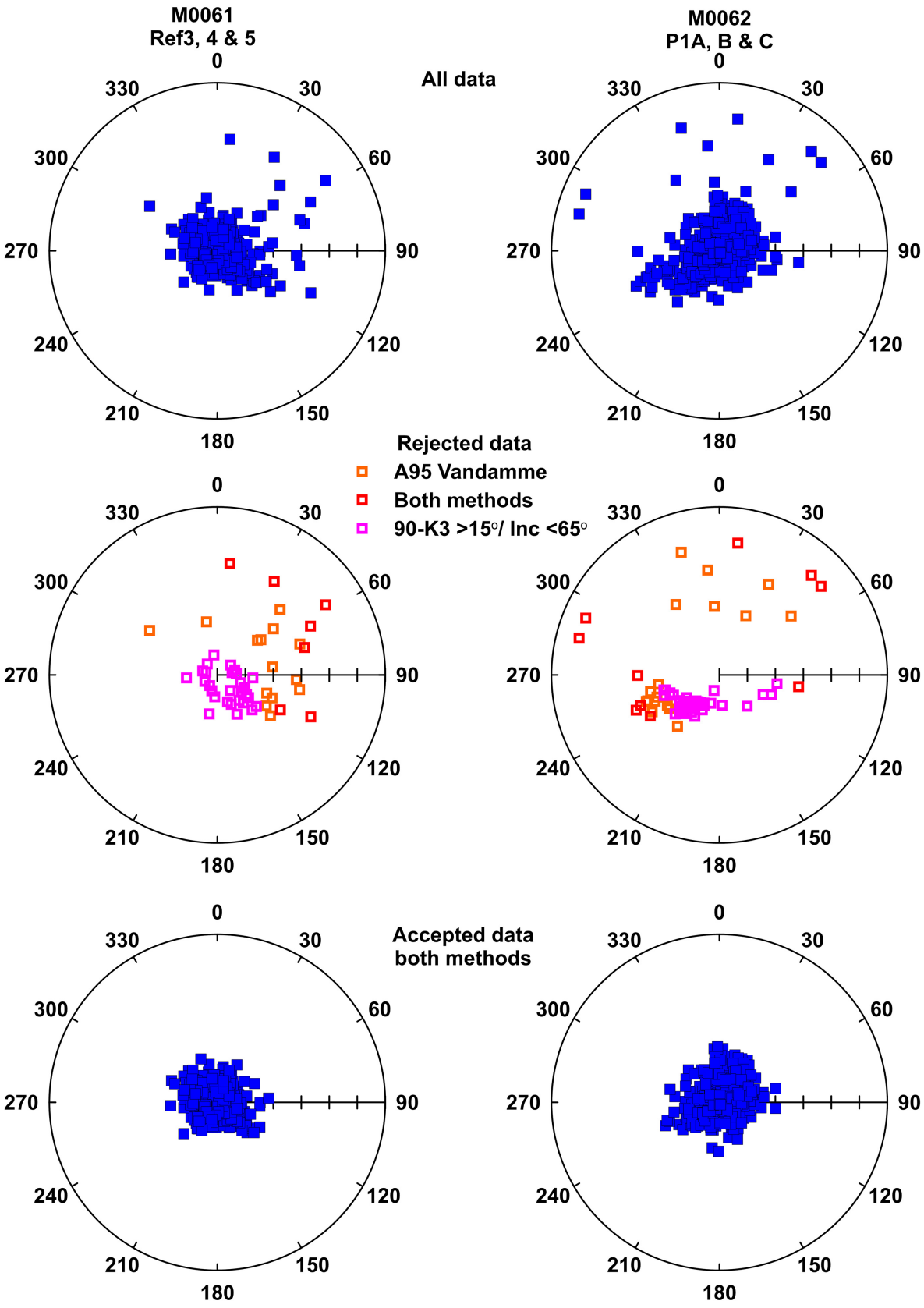

Figure 12. Lower hemisphere, equal area projections that show, for IODP sites M0061 (left) and M0062 (right), the ChRM of the primary data sets obtained from the KPC. The upper projections show the primary data sets. The middle projections show the data points rejected by (i) the statistical method, (ii) the combination of 90-K_3 and a predicted minimum inclination of 65° and (iii) both methods. The lower projections show the data points accepted by both sets of criteria.

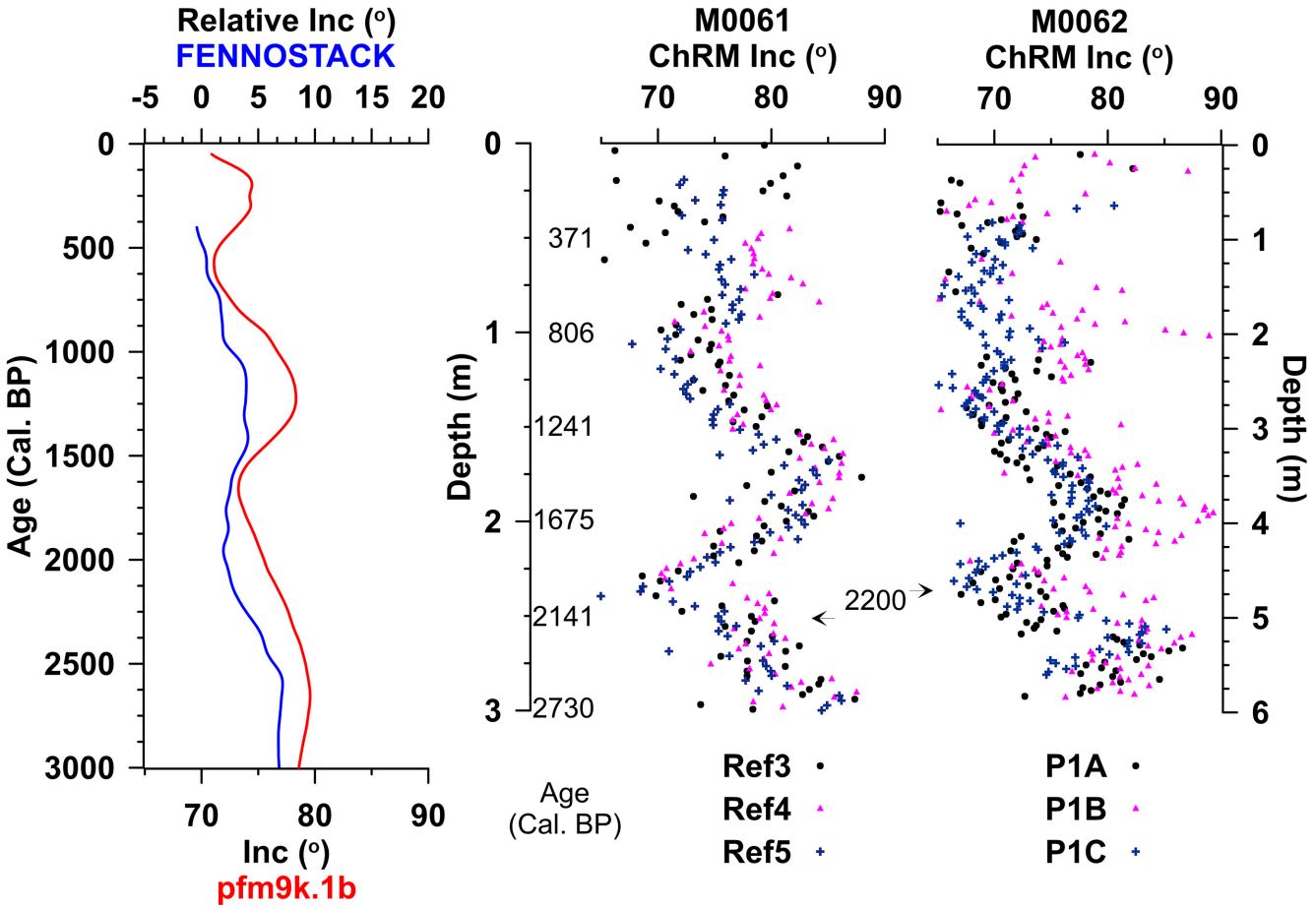

Figure 13. To the left: inclination predicted by the time varying geomagnetic field model pfm9k.1b, which is optimized for sedimentary data (Nilsson *et al.* 2014), and the regional inclination data based on the sedimentary stack FENNOSTACK (Snowball *et al.* 2007). Middle and to the right: accepted ChRM inclination data obtained from the Kullenberg cores plotted against depth. Interpolated ages at 0.5 m increments are shown for site M0061, and are based on the radiocarbon-based age-depth of Dijkstra *et al.* (2018). The positions of a regionally constrained age of ca. 2200 Cal. BP for a peak in *Picea* pollen are also indicated (identified by Warnock *et al.* 2017).

of *Picea* pollen in this region range between 3400 and 3000 Cal. BP, which is consistent (within uncertainties) with our palaeomagnetic data and the radiocarbon-based age model constructed for site M0061.

We note that our inclination features appear older than the predictions of the time-varying geomagnetic field model, but we emphasize that our sedimentary data have not been corrected for any palaeomagnetic lock-in depth that might affect these varved sediments (e.g. Mellström *et al.* 2015). The filtered inclination data stacks from each site appear coherent and, according to the statistical analysis, can be interpreted as a record of past variability in the directions of the geomagnetic vector. Further data analyses, which are outside the scope of this study of AMS and the influence of sampling induced deformation on palaeomagnetic data, are required to independently correlate the IODP sequences to the KPCs, transfer a PSV-based chronology and test the published radiocarbon-based age model for site M0061.

7 CONCLUSIONS

We find that both piston coring methods (APC and KPC) induce artificial AMS fabrics with different intensity, with a consistent artificial AMS induced in the case of the APC system. We are unable to precisely pinpoint the cause of the clear bias of the maximum AMS axis (K_1) parallel to the surfaces of the split APC core sections, but the effect was probably induced by sampling (coring) or core-splitting because subsequent subsampling methods were common to sediment recovered by both corer types. The prolate AMS of the upper sections of Kullenberg cores is most likely due to undersampling ('stretching') of sediment during initial penetration, which has a significant effect on the quality of the palaeomagnetic data (reduced intensity and scattered direction). This stretching effect creates a similar AMS fabric that characterized the upper parts of individual APC core sections that were recovered from M0063 (Landsort Deep) and allowed to expand upwards (Obrochta *et al.* 2017).

We note that AMS measurements cannot be applied to so-called U-channels that are often used to subsample up to 1.5 m lengths of core. On the other hand, X-ray tomography analysis can provide information about internal subsample properties (Tanaka *et al.* 2011) although this method requires more expensive infrastructure. We recommend that AMS data obtained from discrete subsamples are routinely acquired as part of sedimentary palaeomagnetic investigations because they can provide information that is superior to uncertainty parameters derived exclusively from palaeomagnetic data (such as the MAD). We emphasize that our study was carried out on soft sediments such as clays and gyttja-clay, but propose

that the analyses we applied should be routinely used in studies that need to detect disturbing effects of coring systems upon the fabric of other sediment types, such as deep-sea calcareous ooze, which is also regularly subject to palaeomagnetic studies.

ACKNOWLEDGEMENTS

We would like to thank the Scientific crew of IODP Expedition 347 and the crew of the SGU survey vessel (SV) Ocean Surveyor. Anna Svensson assisted with AMS measurements and Matt O'Regan arranged line-scan imaging at Stockholm University and we are grateful to both of them. The work has been partially supported by the Swedish Research Council (VR grant no. 2014-04108). Support for EH-B was provided by the SOEST-HIGP of the University of Hawaii and IODP-USSAC and NSF grants/contracts, and forms publications SOEST#10649 and HIGP#2371. We acknowledge the constructive reviews provided by Anthony Morris and an anonymous reviewer. The lead author (IS) drafted the text, tables and figures. Laboratory measurements were carried out by IS, BL, SW and EH-B. All co-authors contributed to data interpretation and realization of the published article.

REFERENCES

Andrén, T., Jørgensen, B.B., Cotterill, C. & Green, S., Expedition 347 Scientists, 2014. Baltic Sea Basin Paleoenvironment: paleoenvironmental evolution of the Baltic Sea Basin through the last glacial cycle, *IODP Prel. Rept.,* **347,** doi:10.2204/iodp.pr.347.2014.

Andrén, T., Jørgensen, B.B., Cotterill, C. & Green, S., Expedition 347 Scientists, 2015. Baltic Sea paleoenvironment, *Proc IODP, Integrated Ocean Drilling Program,* **347,** doi:10.2204/iodp.proc.347.2015.

Barletta, F., St-Onge, G., Stoner, J.S., Lajeunesse, P. & Locat, J., 2010. A high-resolution Holocene paleomagnetic secular variation and relative paleointensity stack from eastern Canada, *Earth Planet. Sci. Lett.,* **298,** 162–174.

Berglund, M., 2004. Holocene shore displacement and chronology in Ångermanland, eastern Sweden, the Scandinavian glacio-isostatic uplift centre, *Boreas,* **33,** 48–60.

Bowles, J., 2006. Coring-related deformation of Leg 208 sediments from Walvis Ridge: Implications for paleomagnetic data, *Phys. Earth Planet. Inter.,* **161,** 161–169.

Brown, M.C. *et al.*, 2015. GEOMAGIA50.v3: 2. A new paleomagnetic database for lake and marine sediments, *Earth Planets Space,* **67**(1), 1–19.

Cato, I., 1985. The definitive connection of the Swedish geochronological time scale with the present, and the new date of the zero year in Döviken, northern Sweden, *Boreas,* **14**(2), 117–122.

Channell, J.E.T., Mazuad, A., Sullivan, P., Turner, S. & Raymo, M.E., 2002. Geomagnetic excursions and paleointensities in the Matuyama Chron at Ocean Drilling Sites 983 and 984 (Iceland Basin), *J. Geophys. Res.,* **107**(B6), 1–14.

Copons, R., Pares, J.M., Dinares-Turell, J. & Bordonau, J., 1997. Sampling induced AMS in soft sediments: a case study in Holocene glaciolacustrine rhythmites from Lake Barrancs (Central Pyrenees, Spain), *Phys. Chem. Earth,* 137–141.

Deenen, M.H.L., Langereis, C.G., van Hinsbgeren, D.J.J. & Biggin, A., 2011. Geomagnetic secular variation and the statistics of palaeomagnetic directions, *Geophys. J. Int.,* **186,** 509–520.

Dijkstra, N., Quintana Krupinski, N.B., Yamane, M., Obrochta, S.P., Miyairi, Y., Yokoyama, Y. & Slomp, C.P., 2018. Holocene refreshening and reoxygenation of a Bothnian Sea estuary led to enhanced phosphorus burial, *Estuaries Coasts,* **41,** 139–157.

Ekman, M. 1996. A consistent map of the postglacial uplift of Fennoscandia, *Terra Nov.,* **8,** 158–165.

Expedition 347 Scientists, 2015. Site M0063, *Proceedings of the Integrated Ocean Drilling Program,* Vol. **347,** Integr. Ocean Drill. Program Manage. Int., Inc., Edinburgh, Available at http://publications.iodp.org/proceedings/347/347title.htm.

Fisher, R.A., 1953. Dispersion on a sphere, *Proc. R. Soc. Lond.,* **217A,** 295–305.

Gravenor, C.P., Symons, D.T.A. & Coyle, D.A., 1984. Errors in the anisotropy of magnetic susceptibility and magnetic remanence of unconsolidated sediments produced by sampling methods, *Geophys. Res. Lett.,* **1,** 836–839.

Haltia-Hovi, E., Nowaczyk, N. & Saarinen, T., 2010. Holocene palaeomagnetic secular variation recorded in multiple lake sediment cores from eastern Finland, *Geophys. J. Int.,* **180,** 609–699.

Helio, G. & Gillet, N., 2018. Time-correlation-based regression of the geomagnetic field from archeological and sediment records, *Geophys. J. Int.,* **214,** 1585–1607.

Hrouda, F. 1982. Magnetic anisotropy of rocks and its application in Geology and Geophysics, *Surveys in Geophysics,* **5**(1), 37–82.

Hrouda, F. & Kahan, Š., 1991. The magnetic fabric relationship between sedimentary and Basement nappes in the High Tatra Mountains, N. Siovakia, *J. Struct. Geol.,* **13,** 431–442.

Hyttinen, O., Kotilainen, A.T., Virtasalo, J.J., Kekäläinen, P., Snowball, I., Obrochta, S. & Andrén, T., 2016. Holocene stratigraphy of the Ångermanälven river estuary, Bothnian Sea, *Geo Mar. Lett.,* **3,** 273–288.

Jutzeler, M., White, J.D.L., Talling, P.J., McCanta, M., Morgan, S., Le Friant, A. & Ishizuka, O., 2014. Coring disturbances in IODP piston cores with implications for offshore record of volcanic events and the Missoula megafloods, *Geochem. Geophys. Geosyst.,* **15,** 3572–3590.

Kirschvink, J.L., 1980. The least-squares line and plane and the analysis of palaeomagnetic data, *Geophys. J. Int.,* **62,** 699–718.

Koymans, M.R., Langereis, C.G., Pastor-Galan, D. & van Hinsbergen, D.J.J., 2016. Paleomagnetism.org: An online multi-platform open source environment for paleomagnetic data analysis, *Comput. Geosci.,* **93,** 127–137.

Kullenberg, B., 1947. The Piston Core Sampler. Svenska Hydrografiska-Biologiska Rommissionens skrifter, *Tredje Serien: Hydrografl, Band 1, Hafte,* **2,** 1–46.

Le Tirant, P., 1979. *Seabed Reconnaissance and Offshore Soil Mechanics for the Installation of Petroleum Structures,* pp. 508, Editions Technip.

Lougheed, B.C., Nilsson, A., Björck, S., Muscheler, R. & Snowball, I., 2014. A deglacial palaeomagnetic master curve for Fennoscandia - providing a dating template and supporting millennial-scale geomagnetic field patterns for the past 14 ka, *Quat. Sci. Rev.,* **106,** 155–166.

Lund, S.P., Stoner, J. & Lamy, F., 2006. Late Quaternary paleomagnetic secular variation and chronostratigraphy from ODP Sites 1233 and 1234, in *Proc. ODP, Sci. Results, 202,* pp. 1–22, eds Tiedemann, R., Mix, A.C., Richter, C. & Ruddiman, W.F., Ocean Drilling Program, College Station, TX, doi:10.2973/odp.proc.sr.202.208.2006.

Marino, R.J. & Ellwood, BB., 1978. Anomalous magnetic fabric in sediments which record an apparent geomagnetic field excursion, *Nature,* **274,** 581–582.

Mellström, A., Nilsson, A., Stanton, T., Muscheler, R., Snowball, I. & Suttie, N., 2015. Post-depositional remanent magnetization lock-in depth in precisely dated varved sediments assessed by archaeomagnetic field models, *Earth Planet. Sci. Lett.,* **410,** 186–196.

Nilsson, A., Holme, R., Korte, M., Suttie, N. & Hill, M., 2014. Reconstructing Holocene geomagnetic field variation: new methods, models and implications, *Geophys. J. Int.,* **198,** 229–248.

Nowaczyk, N.R., 2003. Detailed study on the anisotropy of magnetic susceptibility of arctic marine sediments, *Geophys. J. Int.,* **152,** 302–317.

Nowaczyk, N.R. & Frederichs, T.W., 1999. Geomagnetic events and relative palaeointensity variations during the past 300 ka as recorded in Kolbeisey Ridge sediments, Iceland, Sea: indication for a strongly variable geomagnetic field, *Int. J. Earth Sci.,* **88,** 116–131.

Obrochta, S.P. *et al.*, 2017. The undatables: Quantifying uncertainty in a highly expanded Late Glacial-Holocene sediment sequence recovered from the deepest Baltic Sea basin—IODP Site M0063, *Geochem. Geophys. Geosyst.,* **18,** 1–18.

Ogg, J.G. & Smith, A.G., 2004. The geomagnetic polarity time scale, in *A Geologic Time Scale,* pp. 63–86, eds Gradstein, F.M., Ogg, J.G. & Smith, A.G., Cambridge Univ. Press.

Panovska, S., Korte, M., Finlay, C.C. & Constable, C.G., 2015. Limitations in paleomagnetic data and modelling techniques and their impact on Holocene geomagnetic field models, *Geophys. J. Int.,* **202,** 402–418.

Parés, J.M., 2015. Sixty years of anisotropy of magnetic susceptibility in deformed sedimentary rocks, *Front. Earth Sci.,* **3,** 4, doi:10.3389/feart.2015.00004.

Potter, D.K. & Stephenson, A., 1988. Single-domain particles in rocks and magnetic fabric analysis, *Geophys. Res. Lett.,* **15,** 1097–1100.

Potter, D.K. & Stephenson, A., 1990. Field-impressed magnetic anisotropy in rocks, *Geophys. Res. Lett.,* **17,** 2437–2440.

Richter, C., Venuti, A., Verosub, K.L. & Wei, K.-Y., 2006. Variations of the geomagnetic field during the Holocene: relative palaeointensity and inclination record from the West Pacific (ODP Hole 1202B), *Phys. Earth Planet. Inter.,* **156,** 179–193.

Rosenbaum, J., Reynold, R., Smoot, J. & Meyer, R., 2000. Anisotropy of magnetic susceptibility as a tool for recognizing core deformation: reevaluation of the paleomagnetic record of Pleistocene sediments from drill hole OL-92, Owens Lake, California, *Earth Planet. Sci. Lett.,* **178,** 415–424.

Räsänen, M.E., Auri, J.M., Huitti, J.V., Klap, A.K. & Virtisala, J.J., 2009. A shift from lithostratigraphic to allostratigraphic classification of Quaternary glacial deposits, *GSA Today,* **19**(2), 4–11.

Sagnotti, L., Macrì, P. & Lucchi, R.G., 2016. Geomagnetic palaeosecular variation around 15 ka ago from NW Barents Sea cores (south of Svalbard), *Geophys. J. Int.,* **204,** 785–797.

Shimono, T., Yamazaki, T. & Inoue, S., 2014. Influence of sampling on magnetic susceptibility anisotropy of soft sediments: comparison between gravity and piston cores, *Earth Planets Space,* **66**(3), 1–8.

Snowball, I., Zillén, L., Ojala, A., Saarinen, T. & Sandgren, P., 2007. FENNOSTACK and FENNORPIS: varve dated Holocene palaeomagnetic secular variation and relative palaeointensity stacks for Fennoscandia, *Earth Planet. Sci. Lett.,* **255,** 106–115.

Stanton, T., Snowball, I., Zillén, L. & Wastegård, S. 2010. Validating a Swedish Varve chronology using radiocarbon, palaeomagnetic secular variation, lead pollution history and statistical correlation, *Quat. Geochronol.,* **5,** 611–524.

Studýnka, J., Chadima, M. & Suza, P., 2014. Fully automated measurement of anisotropy of magnetic susceptibility using 3D rotator, *Tectonophysics,* **629,** 6–13.

Suteerasak, T., Elming, S.-A., Possnert, G., Ingri, J. & Widerlund, A., 2017. Deposition rates and 14C apparent ages of Holocene sediments in the Bothnian Bay of the Gulf of Bothnia using paleomagnetic dating as a reference, *Mar. Geol.,* **383,** 1–13.

Széréméta, N., Bassinot, F., Balut, Y., Labeyrie, L. & Pagel, M., 2004. Oversampling of sedimentary series collected by giant piston corer: Evidence and corrections based on 3.5-kHz chirp profiles, *Paleoceanography,* **19,** PA1005, doi:10.1029/2002PA000795.

Tamaki, M., Suzuki, K. & Fujii, T., 2015. Paleocurrent analysis of Pleistocene turbidite sediments in the forearc basin inferred from anisotropy of magnetic susceptibility and paleomagnetic data at the gas hydrate production test site in the eastern Nankai Trough, *Mar. Pet. Geol.,* **66,** 404–417.

Tanaka, A., Nakano, T. & Ikehara, K., 2011. X-ray computerized tomography analysis and density estimation using a sediment core from the Challenger Mound area in the Porcupine Seabight, off Western Ireland, *Earth Planets Space,* **63,** 103–110.

Tarling, D.H. & Hrouda, F., 1993. *The Magnetic Anisotropy of Rocks,* pp 217, Chapman and Hall.

Tauxe, L., LaBreque, J.L., Dodson, R., Fuller, M. & Dematteo, J., 1983. "U" Channels - a new technique for paleomagnetic analysis of hydraulic piston cores, *EOS, Trans. Am. geophys. Un.,* **64**(18), 219.

Turner, G.M. & Thompson, R., 1981. Lake sediment record of the geomagnetic secular variation in Britain during Holocene times, *Geophys. J. R. Astr. Soc.,* **65,** 703–725.

Vandamme, D., 1994. A new method to determine paleosecular variation, *Phys. Earth Planet. Inter.,* **85,** 131–142.

Vigliotti, L., Channell, J.E.T. & Stockhecke, M., 2014. Paleomagnetism of Lake Van sediments: chronology and paleoenvironment since 350 ka, *Quat. Sci. Rev.,* **104,** 18–29.

Räsänen, M.E., Ojala A.E.K.Virtasalo, J.J., Kotilainen, A.T., 2007. Late-glacial and postglacial deposition in a large, low relief, epicontinental basin: the northern Baltic Sea, *Sedimentology,* 54, 1323–1344.

Warnock, J.P., Buaersachs, T., Kotthoff, U., Brandt, H-T. & Andrén, E., 2017. Holocene environmental history of the Ångermanälven Estuary, northern Baltic Sea, *Boreas,* **47,** 593–608.

SUPPORTING INFORMATION

Supplementary data are available at *GJI* online.

M0061_ChRM_accepted_GJI.docx
M0062_ChRM_accepted_GJI.docx

Please note: Oxford University Press is not responsible for the content or functionality of any supporting materials supplied by the authors. Any queries (other than missing material) should be directed to the corresponding author for the paper.